Little ado about everything. Part II. An 'emergent' dark energy from structure formation to rule cosmic tensions

Andrea Lapi [a,b,c,d,*] Balakrishna S. Haridasu [a,b,*] Lumen Boco [e,a,b]
Marcos M. Cueli [a,b] Carlo Baccigalupi [a,b,c] and Luigi Danese [a,b]

[a] *SISSA,*
Via Bonomea 265, 34136 Trieste, Italy

[b] *Institute for Fundamental Physics of the Universe (IFPU),*
Via Beirut 2, 34014 Trieste, Italy

[c] *INFN-Sezione di Trieste,*
via Valerio 2, 34127 Trieste, Italy

[d] *IRA-INAF,*
Via Gobetti 101, 40129 Bologna, Italy

[e] *Universitat Heidelberg, Zentrum fur Astronomie, Institut fur theoretische Astrophysik,*
Albert-Ueberle-Str. 3, 69120 Heidelberg, Germany

E-mail: lapi@sissa.it, sharidas@sissa.it, lumen.boco@uni-heidelberg.de,
mmunizcu@sissa.it, bacci@sissa.it, danese@sissa.it

ABSTRACT: The ηCDM framework by [1] is a new cosmological model aimed to cure some drawbacks of the standard ΛCDM scenario, such as the origin of the accelerated expansion at late times, the cosmic tensions, and the violation of the cosmological principle due to the progressive development of inhomogeneous/anisotropic conditions in the Universe during structure formation. To this purpose, the model adopts a statistical perspective envisaging a stochastic evolution of large-scale patches in the Universe with typical sizes $10 - 50\,h^{-1}$ Mpc, which is meant to describe the complex gravitational processes leading to the formation of the cosmic web. The stochasticity among different patches is technically rendered via the diverse realizations of a multiplicative noise term ('a little ado') in the cosmological equations, and the overall background evolution of the Universe is then operationally defined as an average over the patch ensemble. In this paper we show that such an ensemble-averaged evolution in ηCDM can be described in terms of a spatially flat cosmology and of an 'emergent' dark energy with a time-dependent equation of state, able to originate the cosmic acceleration with the right timing and to solve the coincidence problem. Moreover, we provide a cosmographic study of the ηCDM model, suitable for quick implementation in the analysis of future observations. Then we test the ηCDM model against the most recent supernova type-Ia, baryon acoustic oscillations and structure growth rate datasets, finding an excellent agreement. Remarkably,

---

*Corresponding author.

we demonstrate that ηCDM is able to alleviate simultaneously both the H_0 and the $f\sigma_8$ tensions. Finally, we discuss that the Linders' diagnostic test could be helpful to better distinguish ηCDM from the standard scenario in the near future via upcoming galaxy redshift surveys at intermediate redshifts such as those being conducted by the Euclid mission.

Contents

1 Introduction

Once upon a time, there was a standard cosmological framework, dubbed ΛCDM, written in stone. In fact, such a model proved extremely successful in the era of precision cosmology, by efficiently reproducing a large number of observations related to the cosmic microwave background (CMB; e.g, [2–5]), type-Ia supernovae (SN; e.g., [6–9]), baryon acoustic oscillations (BAO; e.g., [10–13]), structure growth rates (e.g., [14–19]), galaxy cluster counts (e.g., [20–22]), and many others. However, in recent years the ΛCDM paradigm has been increasingly challenged by new observations and state-of-the-art numerical/theoretical developments.

There are three main, well-recognized downsides of the standard cosmological framework. First, it postulates the existence of a mysterious dark energy component violating the strong energy condition of general relativity, that triggers the accelerated expansion of the Universe at late times (as revealed by type-Ia SN [23, 24] and supported by BAOs) and enforces a closely flat spatial geometry (as required by CMB and BAO data). The observed value of the present-day dark energy density appears weird, being far below any natural scale in particle

physics but surprisingly similar to the current matter density (aka the 'coincidence' problem; e.g., [25, 26]). Recent data from DES and DESI [9, 13], though still debated [27–29], possibly even suggest some form of dynamical dark energy with an evolving equation of state, which may call for an exotic extension of the basic ΛCDM framework.

Second, the ΛCDM model struggles in solving a few cosmic tensions: the H_0 tension concerns the background evolution of the Universe, and highlights a disagreement between the determination of the Hubble constant from late-time observables and the CMB (e.g., [30–32]); the $f\sigma_8$ and $S_8 \equiv \sigma_8 \, (\Omega_m/0.3)^{1/2}$ tensions signal a deficit in these combinations of cosmological parameters (σ_8 being the rms amplitude of the matter power spectrum smoothed on a scale of $8 \, h^{-1}$ Mpc, Ω_m being the matter density, and f being the growth rate of linear perturbations) as constrained from galaxy redshift surveys and cosmic shear data with respect to the CMB expectations (e.g., [33–35]). Of these the H_0 and the $f\sigma_8$ tensions are considered the most serious, since the S_8 tension may be possibly mitigated or explained by baryonic effects (e.g., some form of feedback from astrophysical sources, see [36]).

Third, the ΛCDM model is deeply rooted on the assumption of a homogeneous and isotropic Universe, that allows to adopt a global Friedman-Robertson-Walker metric and to assign a spatially-independent value of the cosmological quantities at any given cosmic time. However, recent data suggest that such an assumption may be questioned at late times on scales $\lesssim 50 \, h^{-1}$ Mpc (and likely on even larger ones, see [37, 38]), that are crucial for several cosmological observables, as well as for the calibration of the cosmic ladder (see [31, 39–41]). Numerical simulations indicate that such violations of isotropy and homogeneity are induced by the complex gravitational processes leading to the formation of the cosmic web, a spider-like network of quasi-linear structures encompassing knots, filaments, walls and voids over a wide range of sizes $R \sim 10 - 50 \, h^{-1}$ Mpc (e.g., [42–44]). Matter flows along the cosmic web structures cause the Universe to be increasingly dominated in volume by voids, and the distribution of overdensities smoothed over scales $\lesssim 50 \, h^{-1}$ Mpc shifts for $z \lesssim 1$ from the initial Gaussian shape to a lognormal one, as expected theoretically (e.g., [45–47]), and inferred observationally from reconstruction of the large-scale velocity field (e.g., [38, 41, 48, 49]).

It is worth mentioning that there are additional open issues, like the nature of DM and the physics of inflation, but these ingredients of the model subtend more successes than doubts (for reviews, see [50, 51]). As to the former, despite the absence for a firm detection of DM particles in colliders or with direct and indirect searches in the sky, the cold DM paradigm (envisaging DM to be constituted by weakly interacting particles that are already non-relativistic at decoupling) explains extremely well the formation of cosmic structures as observed across the history of the Universe. As to the latter, although inflation is still a not perfectly understood physical process, it can solve some fundamental issues like the flatness and the horizon problems, and can provide a natural perspective for understanding the quantum origin of a nearly scale-invariant spectrum of primordial fluctuations. Therefore the standard lore is that the challenge is more on the experimental than on the foundational side (see [52, 53]).

The aforementioned pressing issues, and in particular the origin of the cosmic acceleration, have called for a revision of the standard theory, stimulating the formulation of several cosmological models alternative to it. A non-exhaustive list includes: ab-initio modified

gravity theories with additional degrees of freedom in the matter and/or gravitational action (e.g., [54–56]); phenomenological modifications of the Friedmann equations by non-linear terms in the matter density (Cardassian scenarios; e.g., [57–59]); alteration of the mass-energy conservation equations with bulk viscosity terms (e.g., [60–62]); biases in cosmological parameter estimates due to local underdensities or to the preferential association of standard candles with overdense regions (e.g., [63–65]); deterministic backreaction models highlighting the possible impact of small-scale anisotropies/inhomogeneities in the matter field on the overall cosmic expansion rate (e.g., [66–75]) or stressing the role of voids in providing gravitational energy gradients and variance in clock rates that can be misinterpreted as an apparent dark energy (e.g., the 'timescape' model, see [76–78]). In addition, recent studies in numerical relativity have pointed out that sampling effects associated to the inhomogeneous/anisotropic nature of structure formation could have an appreciable impact on the inference of cosmological observables [79, 80].

Yet no definite paradigm shift has took place, because these alternative theories, despite curing some critical aspects of ΛCDM, are generally more complex (i.e., characterized by more parameters) and do not allow a systematic and coherent performance testing against the exceedingly large amount of available cosmological data (as instead ΛCDM does). As a matter of fact, the excellent performance of the ΛCDM model in coherently reproducing cosmological observations over an extremely wide range of spatial and temporal scales may suggest that any alternative to it should be rather close in terms of phenomenological outcomes, like for example the timing and the strength of the cosmic acceleration, the nearly flat geometry of the Universe, etc. (see [19, 52, 53]); therefore it would be non trivial to perform model selection if not basing on specifically designed diagnostics or convincing theoretical arguments.

Following these lines, in [1] we have proposed a novel model of the Universe dubbed ηCDM that is aimed to cure the aforementioned drawbacks of the standard scenario, at the same time allowing for an extensive testing against several cosmological observables and laying a new theoretical perspective concerning the very foundations of the cosmological landscape. In fact, the ηCDM model drops the deterministic viewpoint underlying the standard 'cosmological principle' (i.e., the statement that the distribution and motion of matter in any sufficiently large spatial region of the Universe are much the same in any other region) and rather adopts a statistical perspective envisaging the evolution of large-scale patches of the Universe as a spatially-stationary stochastic process[1] (i.e., meaning that the probability of the happenings that lead to structure formation in the Universe on sufficiently large scales are similar at every location and in any direction in space). This change of foundational basis was pioneered by [90] and recently advocated by [91] to constitute a possibly crucial step forward in formulating an improved cosmological model of the Universe.

As a consequence, in ηCDM the spatially-averaged evolution of patches with sizes $10 - 50\,h^{-1}$ Mpc includes a degree of scale-dependent stochasticity. Technically, the evolution of the different patches as a function of cosmic time is rendered via the diverse realizations

---

[1]The mathematical framework of stochastic processes is nowadays largely exploited by scientific communities interested in complex systems, especially to describe the formation of spatial and/or temporal structures in physics, chemistry, biology and many other fields (see [81, 82]). In cosmology, the theory of stochastic processes has been applied to investigate inflation (e.g., [83–85]) and to predict the DM halo mass function and related statistics (e.g., [86–89]).

of a multiplicative noise term (a 'little ado') in the mass-energy evolution equation. At any given cosmic time, sampling the ensemble of patches generates a non-trivial distribution of the cosmological quantities; the shape of the noise term is designed in such a way that the overdensity field smoothed on scales $\lesssim 50\,h^{-1}$ Mpc features a closely lognormal distribution, as observed at late times (see references above). The overall behavior of the Universe is then operationally defined as an average over the patch ensemble. Tuning the noise against a wealth of cosmological datasets, in [1] we were able to show that in the ηCDM model an accelerated expansion of the Universe is enforced at late cosmic times, without the need for any postulated dark energy component, while substantially relieving the H_0 tension. The acceleration of the ensemble-averaged evolution originates because, as structure formation proceeds in the Universe, an increasing amount of its volume is statistically occupied by low-density regions (i.e., voids) featuring an enhanced expansion rate (as confirmed by general relativity simulations, see [92]).

In the present work, we further test the ηCDM model against the most recent type-Ia SN, BAO and structure growth rate datasets (including `Pantheon+` and `DESI` samples) to demonstrate that such a framework is able to alleviate simultaneously both the H_0 and the $f\sigma_8$ tensions. We also offer a new look to the ηCDM model, showing that its ensemble-averaged evolution can be rendered in terms of a spatially flat cosmology and of an emergent dark energy component with a time-dependent equation of state. In addition, we also provide a new cosmographic analysis of the ηCDM model, suitable for quick implementation in the analysis of future datasets.

The plan of the paper is as follows. In section 2 we briefly recap the basics of the ηCDM model and provide the aforementioned novel theoretical viewpoint. In section 3 we describe the datasets, detail our analysis and present our results. In section 4 we discuss our main findings. In section 5 we summarize the present work, drawing general conclusions and outlining future perspectives.

2 A primer of the ηCDM model

In this section we first briefly recap the basics of the ηCDM model as presented in [1], and then provide a novel look at it, showing that the ensemble-averaged evolution of the Universe in such a framework can be rendered as a spatially flat cosmology equipped with an 'emergent' dark energy component.

2.1 Basics

The foundational change of paradigm at the hearth of the ηCDM model is to drop the classic deterministic formulation of the cosmological principle, and to adopt instead a statistical perspective envisaging the evolution of large-scale patches of the Universe as a spatially-stationary stochastic process. In other words, when smoothed on scales $10 - 50\,h^{-1}$ Mpc pertaining to the formation of the cosmic web, cosmological quantities are not assumed to take the same value at any location (dependent only on time, like in the standard theory), but rather to take different values at different locations according to well-definite probability distributions (with these dependent on time but independent of position and or orientation). This view is largely supported by numerical simulations and observations of the smoothed density field

(see references in section 1; also appendix A). In fact, the latter's distribution follows an approximately Gaussian shape at early times reflecting the initial conditions, and becomes progressively lognormal at late times; this is due to the complex gravitational processes associated to structure formation which tend to aggregate matter in the filaments/nodes of the cosmic web, while subtracting it from other regions that will become the voids.

Thus in ηCDM the evolution of different large-scale patches in the Universe with sizes $10-50\,h^{-1}$ Mpc includes a degree of stochasticity, which is rendered via the diverse realizations of a multiplicative noise term in the cosmological equations, promoting these to a stochastic differential system

$$
\begin{cases}
H^2 = \dfrac{8\pi G}{3}\left(\rho_m + \rho_\gamma\right) - \dfrac{k}{a^2}\,, \\[2ex]
\dot{\rho}_{m,\gamma} = -3H\,\rho_{m,\gamma}\left(1 + \omega_{m,\gamma}\right) + \zeta\,\rho_{m,\gamma}\,H^\alpha\,H_\star^{-\alpha+1/2}\,\eta(t)\,;
\end{cases}
\tag{2.1}
$$

here a is the scale factor, $H \equiv \dot{a}/a$ the Hubble rate, k the curvature constant, $\rho_{m,\gamma}$ the matter and radiation densities with $(\omega_m, \omega_\gamma) = (0, 1/3)$; moreover, $\eta(t)$ is a Gaussian white noise of the Stratonovich type with ensemble-average statistical properties $\overline{\eta(t)} = 0$ and $\overline{\eta(t)\eta(t')} = 2\,\delta_{\mathrm{D}}(t - t')$, $\zeta > 0$ and $\alpha < 0$ are two parameters regulating the strength and redshift dependence of the noise,[2] and $H_\star = 100$ km s^{-1} Mpc^{-1} is a reference value of the Hubble rate that is present for dimensional consistency (since η has dimension of one over square root of time). We stress that the above equations refer to patches of the Universe with a given size $10 - 50\,h^{-1}$ Mpc and that the quantities appearing there are spatially-averaged (i.e., smoothed) over such a scale. Thus if we imagine to tessellate the Universe with these patches, each realization of the noise $\eta(t)$ will correspond to a slightly different evolution for each patch. At any given cosmic time, sampling the ensemble of patches will originate a non-trivial distribution of the smoothed cosmological quantities. The evolution of the Universe as a whole is operationally defined as the ensemble-average over the different patches.

In appendix A the form of these equations for the matter component is shown to emerge quite naturally from a spatial-averaging procedure in Newtonian cosmology.[3] Moreover, there it is shown that the strength of the noise $\zeta \propto \langle\theta^2\rangle$ can be related to the spatially-averaged variance of the peculiar velocity field divergence $\theta \equiv \nabla\cdot\dot{\mathbf{x}}$, and that there are good arguments to expect an evolution parameter $\alpha \gtrsim -1$. Given that the stochasticity is associated to structure formation, on very large scales and/or at early times the impact of the noise will be negligible and the average evolution of the Universe will be indistinguishable from the standard ΛCDM scenario. However, as already mentioned in section 1 there are robust

---

[2]Note that in principle the noise terms in the matter and radiation components could feature different shapes (e.g., different parameters ζ and α), but here for the sake of simplicity we have assumed similar expressions for them, though each one is proportional to the corresponding energy density $\rho_{m,\gamma}$. In fact, this proportionality makes any specific assumption on the noise term in the radiation component irrelevant since at late times when noise becomes important ρ_γ is negligible, while toward high redshift when ρ_γ becomes appreciable the noise is suppressed (since $\alpha < 0$ and H grows).

[3]Note that for notational economy in the above equations we have dropped the symbols $\langle\cdot\rangle$ used in the appendix to denote spatial averaging, but every quantity is meant to be smoothed on a given spatial scale. In the same vein, we have indicated with ρ the density source although in appendix A it is shown that this should be an effective quantity ρ_{eff} including a sub-leading contribution from the noise itself; in our framework $\rho_{\mathrm{eff}} \approx \rho$ since the noise describes only small deviation from homogeneity/isotropy.

evidences from observations and from numerical simulations that appreciable values of $\langle\theta^2\rangle$ applies at late times on scales of several tens Mpc associated to the emergence of the cosmic web, that are actually quite critical for many cosmological data, such as the calibration of the cosmic ladder (e.g., [41, 49]). Thus it is natural to expect that the stochasticity will induce some non-trivial effects on the late-time evolution of the Universe, at least when this is operationally defined as an ensemble-average over different patches with such a size. Note that the impact of adding a phenomenological noise term in the evolution of perturbations due to gravitational instability has been previously considered by [93].

To proceed, it is convenient to introduce the normalized Hubble rate $h \equiv H/H_\star$, the normalized time $\tau \equiv H_\star t$ so that $\eta(\tau) = \eta(t)/\sqrt{H_\star}$ applies, and the density parameters $\Omega_{m,\gamma} \equiv 8\pi G \rho_{m,\gamma}/3H^2$. In this way we can put the equations above in the adimensional form:

$$
\begin{cases}
\dot{h} = h^2 \left(-1 - \dfrac{\Omega_m}{2} - \Omega_\gamma\right) + \dfrac{\zeta}{2}\left(\Omega_m + \Omega_\gamma\right) h^{\alpha+1} \eta(\tau), \\[2mm]
\dot{\Omega}_m = \Omega_m\, h\left(-1 + \Omega_m + 2\,\Omega_\gamma\right) + \zeta\left(1 - \Omega_m - \Omega_\gamma\right)\Omega_m\, h^\alpha \eta(\tau), \\[2mm]
\dot{\Omega}_\gamma = \Omega_\gamma\, h\left(-2 + \Omega_m + 2\,\Omega_\gamma\right) + \zeta\left(1 - \Omega_m - \Omega_\gamma\right)\Omega_\gamma\, h^\alpha \eta(\tau),
\end{cases} \tag{2.2}
$$

where overdot means now differentiation with respect to τ. In [1] we have shown that the evolution of the Universe implied by these stochastic equations includes a dominant ensemble-averaged component common to all the patches, plus a small random component superimposed to it that make the evolution of each patch slightly different from the others. In the present work we are only concerned with the ensemble-averaged evolution. To a first approximation this can be easily derived from the Kramers-Moyal drift and diffusion coefficients associated to the stochastic system (see [1] for details). Specifically, for a generic set of equations for the variables $\xi \equiv \{\xi_i\}$ subject to Stratonovich-type noise of the form $\dot{\xi}_i = f_i(\xi) + g_{ij}(\xi)\,\eta_j(t)$, the ensemble-averaged deterministic components $\{\bar{\xi}_i\}$ are approximately given by $\dot{\bar{\xi}}_i = f_i(\bar{\xi}) + g_{kj}\,\partial_k\,g_{ij}(\bar{\xi})$; the second addenda represents a noise-induced drift that come from the multiplicative nature of the stochasticity. In the present context we get:

$$
\begin{cases}
\dot{\bar{h}} = \bar{h}^2 \left(-1 - \dfrac{\bar{\Omega}_m}{2} - \bar{\Omega}_\gamma\right) + \dfrac{\zeta^2}{2}(\bar{\Omega}_m + \bar{\Omega}_\gamma)\,\bar{h}^{2\alpha+1}\left[1 - \dfrac{1-\alpha}{2}(\bar{\Omega}_m + \bar{\Omega}_\gamma)\right], \\[3mm]
\dot{\bar{\Omega}}_m = \bar{\Omega}_m\,\bar{h}\left(-1 + \bar{\Omega}_m + 2\,\bar{\Omega}_\gamma\right) + \zeta^2\left(1 - \bar{\Omega}_m - \bar{\Omega}_\gamma\right)\bar{\Omega}_m\,\bar{h}^{2\alpha}\left[1 - \dfrac{4-\alpha}{2}(\bar{\Omega}_m + \bar{\Omega}_\gamma)\right], \\[3mm]
\dot{\bar{\Omega}}_\gamma = \bar{\Omega}_\gamma\,\bar{h}\left(-2 + \bar{\Omega}_m + 2\,\bar{\Omega}_\gamma\right) + \zeta^2\left(1 - \bar{\Omega}_m - \bar{\Omega}_\gamma\right)\bar{\Omega}_\gamma\,\bar{h}^{2\alpha}\left[1 - \dfrac{4-\alpha}{2}(\bar{\Omega}_m + \bar{\Omega}_\gamma)\right],
\end{cases} \tag{2.3}
$$

which are the basic equations of the ηCDM model derived in [1]. Hereafter the bar over the variables is omitted for notational economy, but we stress that all the quantities are ensemble-averaged.

2.2 An 'emergent' dark energy

We now innovate with respect to [1] by taking a more convenient and transparent route. First, we combine the above equations to obtain

$$2\frac{\dot{h}}{h} + 2h - \frac{3}{2}\zeta^2 h^{2\alpha}(\Omega_m + \Omega_\gamma)^2 = \frac{\dot{\Omega}_m + \dot{\Omega}_\gamma}{1 - \Omega_m - \Omega_\gamma};\qquad(2.4)$$

then we integrate in time to derive the ensemble-averaged analogue of the Friedmann constraint

$$\Omega_\eta \equiv -\frac{\kappa}{h^2\,a^2}\, e^{\frac{3}{2}\zeta^2\int_0^\tau \mathrm{d}\tau\, h^{2\alpha}(\Omega_m + \Omega_\gamma)^2} = 1 - \Omega_m - \Omega_\gamma\,,\qquad(2.5)$$

where κ is a constant of integration and Ω_η is a dark energy-like term 'emergent' from the noise. In terms of the latter, the ensemble-average Universe is formally equivalent to a flat cosmology with $\Omega_m + \Omega_\gamma + \Omega_\eta = 1$.

To interpret κ in physical terms we may note that in the early Universe the effect of the noise is negligible (the integral in the argument of the exponential vanishes) and the emergent dark energy behaves like a standard curvature component since $\Omega_\eta \simeq -\kappa/h^2\,a^2$ applies. In fact, in the closely homogeneous/isotropic primordial patches of the Universe, the constant $k \propto \langle\mathcal{R}\rangle$ appearing in equations (2.1) is directly linked to the spatially-averaged scalar curvature $\langle\mathcal{R}\rangle$ of the patch (see equation (A.12)), and thus κ could be safely identified at early times with an ensemble-averaged spatial curvature constant. For equation (2.5) to be consistent at late times the κ is bound to be negative since $1 - \Omega_{m,0} - \Omega_{\gamma,0} > 0$. This implies that the ensemble-averaged spatial curvature in the early Universe must also be negative, though it can be arbitrarily small (this is allowed since $\kappa/h^2\,a^2$ tends to zero toward the Big Bang when $1 - \Omega_m - \Omega_\gamma$ is tiny), so as not to violate cosmological data [5]; however, if initially it is exactly zero, then $\kappa = 0$ so that Ω_η will stay null and no emergent dark energy will be originated, even when the noise term is present. At late times the direct proportionality between k and the spatially-averaged scalar curvature $\langle\mathcal{R}\rangle$ of the patch is broken, since also inhomogeneities/anisotropies due to structure formation can develop curvature in general relativity (see equation (A.12)), a positive one in the filaments/sheets of the cosmic web and a negative one in the voids. However, when ensemble-averaging over all the patches, it is plausible to expect that the original small overall curvature has not been substantially altered, and that the ensemble-averaged Universe will stay close to flatness. In this perspective of ensemble-averaged evolution, the exponential term in equation (2.5) effectively acts in transforming a small curvature term at early epochs into an emergent dark energy at late times.

Nevertheless, other interpretations are possible. For example, in [1] we took an alternative viewpoint by writing equation (2.5) in the form of a modified Friedman constraint $\Omega_\kappa \equiv -\kappa/h^2\,a^2 = (1 - \Omega_m - \Omega_\gamma)\,e^{-3\zeta^2/2\int \mathrm{d}\tau\, h^{2\alpha}(\Omega_m + \Omega_\gamma)^2}$, so that one can interpret Ω_κ as an emergent (negative) curvature-like component with a non-standard evolution. To fit cosmological data, in [1] we found that Ω_k is bound to be small in the remote past, to grow at a maximal value $\Omega_k \lesssim 0.1$ at late times, and then to vanish again in the infinite future; at variance with the standard cosmology, and thanks to the exponential term related to the noise, Ω_k is allowed to stay relatively small even if $1 - \Omega_m$ increases toward late times, thus never dominating the cosmic energy budget (see figure 4 in [1]). However, in this interpretation the

definition of distances in the ensemble-averaged cosmology is somewhat problematic, since the curvature component features a non-standard evolution and its relationship with an overall ensemble-averaged metric is non-trivial. In any case, the above discussion is reminiscent of deterministic backreaction models in a general relativistic setting, where the concepts of an emergent dark energy and an emergent curvature are often identified, as pioneered by [68, 69] and numerically demonstrated by [94].

We also note that the ηCDM model correctly reproduces as limiting cases the expected behavior in absence of the noise ($\zeta \approx 0$) or in a Milne's Universe devoid of matter/radiation components ($\Omega_{m,\gamma} \approx 0$). In both cases the exponential in equation (2.5) goes to unity, so that the emergent dark energy is just standard curvature ($\Omega_\eta = \Omega_k$) and the evolution closely resembling an Einstein de Sitter (with $\Omega_m \approx 1$ and $\Omega_\kappa \approx 0$) or a purely (anti-)de Sitter Universe (with $\Omega_m \approx 0$ and $\Omega_\kappa \approx 1$) is recovered.

We have still to better justify the name 'dark energy' for the component Ω_η defined above by deriving its equation of state. To this purpose it is instructive to rewrite all the original equations in terms of the triple $(h, \Omega_m, \Omega_\eta)$ by eliminating $\Omega_\gamma = 1 - \Omega_m - \Omega_\eta$. After some algebraic manipulations, we get

$$
\begin{cases}
\dot{h} = h^2 \left(-2 + \dfrac{\Omega_m}{2} + \Omega_\eta \right) + \dfrac{\zeta^2}{2} (1 - \Omega_\eta) \, h^{2\alpha+1} \left[1 - \dfrac{1-\alpha}{2} (1 - \Omega_\eta) \right] \\[2mm]
\dot{\Omega}_m = \Omega_m \, h \, (1 - \Omega_m - 2\,\Omega_\eta) + \zeta^2 \, \Omega_m \, \Omega_\eta \, h^{2\alpha} \left[1 - \dfrac{4-\alpha}{2} (1 - \Omega_\eta) \right] \\[2mm]
\dot{\Omega}_\eta = \Omega_\eta \, h \, (2 - \Omega_m - 2\,\Omega_\eta) - \zeta^2 \, \Omega_\eta \, (1 - \Omega_\eta) \, h^{2\alpha} \left[1 - \dfrac{4-\alpha}{2} (1 - \Omega_\eta) \right] .
\end{cases}
\tag{2.6}
$$

We notice that at late times when structure formation develops, $\Omega_\eta \simeq 1 - \Omega_m$ and $\dot{\Omega}_\eta \simeq -\dot{\Omega}_m$ apply, consistently with the above equations. Now using $\dot{\rho}/\rho = (\dot{\Omega}/\Omega) + 2\,(\dot{h}/h) = -3\,h\,(1+w)$ we obtain:

$$
\begin{cases}
w_m = -\dfrac{\zeta^2}{3} h^{2\alpha-1} \left[1 - \dfrac{1-\Omega_\eta}{2} (3\Omega_\eta + 1 - \alpha) \right] \simeq -\dfrac{\zeta^2}{6} h^{2\alpha-1} \left[2 - (4-\alpha)\,\Omega_m + 3\,\Omega_m^2 \right] , \\[2mm]
w_\eta = -\dfrac{1}{3} - \dfrac{\zeta^2}{2} h^{2\alpha-1} (1-\Omega_\eta)^2 \simeq -\dfrac{1}{3} - \dfrac{\zeta^2}{2} h^{2\alpha-1} \Omega_m^2 ,
\end{cases}
\tag{2.7}
$$

with the second expressions holding at late times when a non-zero $\Omega_\eta \simeq 1 - \Omega_m$ applies. The first point to notice is that Ω_η features an equation of state $w_\eta \leq -1/3$ at all times, and so always tends to induce an accelerating behavior, justifying its name as emergent dark energy. As described earlier $w_\eta \to -1/3$ holds at early times to resemble a small curvature-like component before the noise term kicks in to enforce acceleration.

Moreover, the noise also alters the matter equation of state, which starts with the usual $w_m \approx 0$ at early times (i.e., pressureless dust), but progressively lowers toward $w_m \lesssim -1/3$ at late times. We stress that the modification of the matter equation of state is just apparent: the ηCDM model relies on the standard cold DM scenario, and the intrinsic properties of the particles will plainly not be affected by the stochasticity. The matter equation of state changes since one insists to describe the ensemble-averaged energy density evolution in terms

of a standard mass-energy conservation equation. The negative w_m here just means that the dilution due to cosmic expansion for the ensemble-averaged matter density becomes slower than the standard trend.

This often occurs in cosmological models with strong coupling in the dark sector (e.g., [95–102]): in fact, the noise term in the last two equations (2.6) can be viewed as describing a very specific form of dark coupling. In particular, such a noise-driven interaction makes an equal and opposite contribution to the evolution of Ω_m and Ω_η, and renders a kind of energy transfer from DM to the emergent dark energy or viceversa, depending on its sign. At sufficiently high redshift when $\Omega_m \gtrsim 2/(4-\alpha)$ there is a net energy transfer from DM to dark energy (related to voids expanding fast and rapidly tending to dominate the Universe in volume), that actually reinforces the lowering of Ω_m and the rise of Ω_η with respect to the case without noise. At later times instead when $\Omega_m \lesssim 2/(4-\alpha)$ the situation is reversed (matter clustering proceeds along the structure of the cosmic web while void expansion progressively stalls since almost all the volume has been occupied) so that the evolution of the two components Ω_m and Ω_η considerably slows down, to the point of asymptotically saturating in the future (see also section 2.4).

2.3 ηCDM cosmography

The cosmological evolution at late times in the ηCDM model can be better discerned by inspecting the cosmographic parameters. The deceleration parameter q is routinely defined as

$$q \equiv -\frac{\ddot{a}\,a}{\dot{a}^2} = -1 - \frac{\dot{h}}{h^2}\,. \tag{2.8}$$

At late times, its expression in the ηCDM model is explicitly given by

$$q_{\eta\mathrm{CDM}} = \frac{\Omega_m}{2} - \frac{\zeta^2}{2}\,\Omega_m\,h^{2\alpha-1}\left(1 - \frac{1-\alpha}{2}\,\Omega_m\right); \tag{2.9}$$

for $\alpha \gtrsim -1$, $\zeta \sim 1$ of order unity and reasonable values of h_0 and $\Omega_{m,0}$, an accelerated expansion with the observed $q_0 \lesssim -0.5$ can be easily obtained. For reference, in ΛCDM $q_{\Lambda\mathrm{CDM}} = -1 + 3\,\Omega_m/2$.

At higher-order, the jerk is defined as

$$j \equiv \frac{\dddot{a}\,a^2}{\dot{a}^3} = 1 + 3\,\frac{\dot{h}}{h^2} + \frac{\ddot{h}}{h^3} = q + 2\,q^2 - \frac{\dot{q}}{h} \tag{2.10}$$

and its expression in ηCDM reads

$$
\begin{aligned}
j_{\eta\mathrm{CDM}} = \Omega_m\Bigg\{ &1 - \frac{\zeta^2}{8}\,h^{2\alpha-1}\Big[8(1+\alpha) + 2\left(-7+3\alpha+2\alpha^2\right)\Omega_m + \left(9-5\alpha+2\alpha^2\right)\Omega_m^2\Big] \\
&+ \frac{\zeta^4}{16}\,h^{4\alpha-2}\Big[8 + 4(-7+5\alpha)\Omega_m + 12\left(3-3\alpha+\alpha^2\right)\Omega_m^2 + \left(-15+20\alpha-7\alpha^2+2\alpha^3\right)\Omega_m^3\Big]\Bigg\};
\end{aligned} \tag{2.11}
$$

for reference, in ΛCDM $j_{\Lambda\mathrm{CDM}} = 1$.

In addition, the snap is defined as

$$s \equiv \frac{\ddddot{a}\,a^3}{\dot{a}^4} = 1 + 6\,\frac{\dot{h}}{h^2} + 4\,\frac{\ddot{h}}{h^3} + \frac{3\dot{h}^2 + \dddot{h}}{h^4} = -2j - 3q\,j + \frac{\dot{j}}{h} \tag{2.12}$$

– 9 –

and its expression in ηCDM reads

$$
\begin{aligned}
s_{\eta\text{CDM}} = \Omega_m \Bigg\{ &-3 - \frac{\Omega_m}{2} + \frac{\zeta^2}{8}\, h^{2\alpha-1} \Bigg[(24 + 32\alpha + 16\alpha^2) + 2\,(-27 + \alpha + 16\alpha^2 + 4\alpha^3)\,\Omega_m \\
&+ (60 - 20\alpha + 8\alpha^3)\,\Omega_m^2 + (-18 + 19\alpha - 9\alpha^2 + 2\alpha^3)\,\Omega_m^3 \Bigg] - \frac{\zeta^4}{32}\, h^{4\alpha-2} \Bigg[(48 + 96\alpha) \\
&+ (-296 - 80\alpha + 240\alpha^2)\,\Omega_m + 8\,(92 - 45\alpha - 18\alpha^2 + 18\alpha^3)\,\Omega_m^2 + (-784 + 754\alpha \\
&- 210\alpha^2 + 24\alpha^3 + 24\alpha^4)\,\Omega_m^3 + (303 - 364\alpha + 221\alpha^2 - 64\alpha^3 + 12\alpha^4)\,\Omega_m^4 \Bigg] \\
&+ \frac{\zeta^6}{64}\, h^{6\alpha-3} \Bigg[32 + (-304 + 240\alpha)\,\Omega_m + 16\,(69 - 78\alpha + 26\alpha^2)\,\Omega_m^2 + 4\,(-471 \\
&+ 636\alpha - 319\alpha^2 + 70\alpha^3)\,\Omega_m^3 + 2\,(759 - 1156\alpha + 693\alpha^2 - 228\alpha^3 + 40\alpha^4)\,\Omega_m^4 \\
&+ (-465 + 785\alpha - 497\alpha^2 + 219\alpha^3 - 50\alpha^4 + 8\alpha^5)\,\Omega_m^5 \Bigg] \Bigg\} ;
\end{aligned}
\tag{2.13}
$$

for reference, in ΛCDM $s_{\Lambda\text{CDM}} = 1 - 9\,\Omega_m/2$.

If one inserts in equations (2.9)–(2.11)–(2.13) the matter density parameter $\Omega_m(z)$ and the Hubble rate $h(z)$ as a function of redshift obtained by solving the system of equations (2.6), then the deceleration, jerk and snap parameters at any epochs are directly obtained (only requirements is that radiation energy density is small, and we have checked that this implies a range of validity $z \lesssim 30$). On the other hand, from the same equations above one can compute q_0, j_0 and s_0 at $z \approx 0$ as a function of the present matter density $\Omega_{m,0}$, Hubble constant h_0 and of the noise parameters ζ and α.

These can in turn be exploited to obtain cosmographic approximations at low redshift $z \lesssim 0.5$ for the Hubble rate and the luminosity distance[4] (e.g., [105, 106]). Specifically, one has:

$$
h(z) \simeq h_0 \left[1 + y\,(1+q_0) + \frac{y^2}{2}\,(2 + j_0 + 2q_0 - q_0^2) + \frac{y^3}{6}\,(6 + 6q_0 - 3q_0^2 + 3q_0^3 + 3j_0 - 4j_0q_0 - s_0) \right],
\tag{2.14}
$$

and

$$
\begin{aligned}
d_L(z) \simeq \frac{c}{H_0}\, y \Bigg[1 &+ \frac{y}{2}\,(3 - q_0) + \frac{y^2}{6}\,(11 - 5q_0 + 3q_0^2 - j_0) \\
&+ \frac{y^3}{24}\,(50 - 26q_0 + 21q_0^2 - 15q_0^3 - 7j_0 + 10j_0q_0 + s_0) \Bigg],
\end{aligned}
\tag{2.15}
$$

where $y \equiv z/(1+z)$. From the latter expression the proper distance $d_M = d_L/(1+z)$ and the angular diameter distance $d_A = d_L/(1+z)^2$ can be easily derived. These analytic expressions can be useful for the future analysis of cosmological datasets.

---

[4]Since the inhomogeneities/anisotropies described by the noise term are expected to be small, it is a reasonable approximation to assume that the ensemble-averaged Universe is described by a Friedman-Robertson-Walker metric, and to adopt the standard redshift-distance relation [103, 104].

2.4 Fate of the Universe and coincidence problem

Remarkably, in the infinite future the ensemble-averaged evolution in ηCDM features an attractor solution, that can be found by setting $\dot{h} = \dot{\Omega}_m = \dot{\Omega}_\eta \approx 0$ in equations (2.6), to yield

$$\begin{cases} \Omega_{m,\infty} = \dfrac{\alpha - 4 + \sqrt{(\alpha - 4)^2 + 12}}{3}\,, \\[2ex] \Omega_{\eta,\infty} = 1 - \Omega_{m,\infty}\,, \\[2ex] h_\infty = \left[\zeta^2 \left(1 - \dfrac{4 - \alpha}{2}\,\Omega_{m,\infty}\right)\right]^{\frac{1}{1-2\alpha}}\,; \end{cases} \tag{2.16}$$

in addition one can show from equations (2.7) that $w_m \approx w_\eta \approx -1$, $q_\infty \approx -1$, $j_\infty \approx 1$ and $s_\infty \approx 1$. To some extent, the noise will originate a kind of inflationary behavior in the infinite future, with all the relevant components behaving like a cosmological constant, i.e. featuring a constant energy density. Note that the condition $\Omega_m < 2/(4 - \alpha)$ must hold at late cosmic times for the third expression above to be meaningful, and for this attractor solution to set in. As already mentioned in section 2.2, the presence of this attractor solution at late times can be traced back to a kind of equilibrium in the energy exchange between Ω_m and Ω_η, or in more physical terms between the clustering of matter along the structures of the cosmic web and the increasing dominance in volume by the voids.

As also pointed out in [1], it is easy to check that for $\alpha \gtrsim -1$ and $\zeta \sim 1$ the cosmological parameters will hover around values similar to the current ones for an infinite amount of time in the future. This is strongly at variance with many other cosmological models, where the matter and dark energy densities have an opposite trend with cosmic time (e.g., in ΛCDM one has $\Omega_m \approx 1$ and $\Omega_\Lambda \approx 0$ in the remote past while $\Omega_m \approx 0$ and $\Omega_\Lambda \approx 1$ in the infinite future), thus bringing about the cosmic coincidence issue of why nowadays these quantities have similar values. In ηCDM, given that the present values will stay put for an infinite amount of time in the future, the cosmic coincidence is solved without recurring to anthropic considerations, apart from the trivial fact that a human being must be here and now to raise such an issue.

2.5 ηCDM vs. ΛCDM evolution

In figure 1 we illustrate the evolution with redshift of various relevant quantities in the ηCDM model, and compare them with the analogous ones in ΛCDM. For ηCDM these outcomes are obtained just by integrating equations (2.6) backward in time from given initial conditions at the present epoch. Specifically, we choose the set of cosmological parameters $h_0 \approx 0.7$, $\Omega_{m,0} \approx 0.4$, $\zeta \approx 1.5$, $\alpha \approx -0.75$ that will turn out to fit quite well cosmological observables (see section 3.2). For the sake of definiteness, in ΛCDM we adopt the `Planck` bestfits [5].

It is seen that the expansion rate, the energy densities, timescales, distances are very similar in the two models, with the main deviations occurring at late times when the noise becomes important. Perhaps the most striking difference can be identified in the evolution of the equation of state for the dark energy component, which is varying with redshift in ηCDM, while it is constant $w_\Lambda \approx -1$ in ΛCDM (at least in its basic version). This is an occurrence that could be tested by the `Euclid` mission via weak lensing and galaxy clustering analysis. We also highlight the appreciably different evolutions of the cosmographic
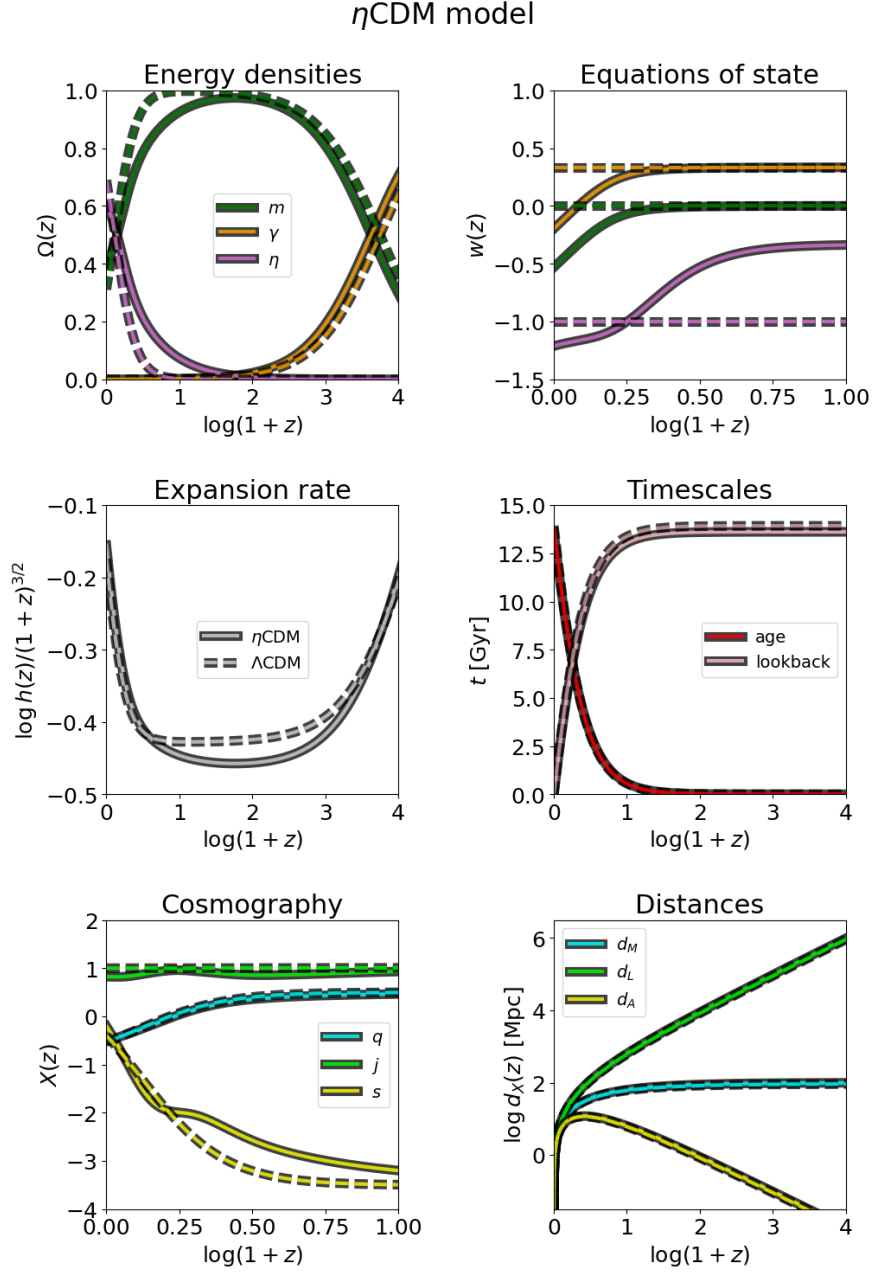
Figure 1. Ensemble-averaged evolution of the Universe in the ηCDM model (solid lines). The different panels illustrate the energy densities (top left), equations of state (top right), expansion rate (middle left), timescales (middle right), cosmographic quantities (bottom left) and cosmological distances (bottom right). In the top panels, green lines refer to matter, orange lines to radiation and magenta lines to the (emergent) dark energy; in the middle right panel pink line shows the lookback time and red line shows the age of the Universe; in the bottom left panel, cyan lines show the deceleration parameter q, green lines show the jerk parameter j and yellow lines the snap parameter s; in the bottom right panel, cyan lines show the transverse comoving distance d_M, green line the luminosity distance d_L and yellow lines the angular distance d_A. In all panels the standard ΛCDM model (dashed lines) is also reported for reference.

parameters at intermediate to high z, especially the jerk and the snap. These could provide independent tests to be performed via searches for transient objects (e.g., supernovae) with future surveys like those planned on the `Nancy Grace Roman Space Telescope`. Another potentially interesting diagnostics to differentiate the two models concerns the growth rate of cosmic structures vs. that of the background, and will be discussed in section 4.2.

3 Tuning noise and fitting data

We will now turn to set the parameters of the ηCDM model and to investigate its overall performance in reproducing a wealth of recent cosmological observations.

3.1 Data and analysis

We focus on the following datasets:

- *Baryon acoustic oscillations (BAO).* We exploit the `DESI` BAO sample of 7 measurements in the redshift range $z \sim 0.1 - 4$ by [13] to fit for the ratios d_M/r_d, d_H/r_d and d_V/r_d between the transverse comoving distance

$$d_M(z) = c \int_0^z \frac{\mathrm{d}z'}{H(z')}, \tag{3.1}$$

the Hubble distance $d_H(z) = c/H(z)$ and the angle-averaged distance $d_V(z) = [z\, d_M^2\, d_H]^{1/3}$ to the scale of the drag epoch sound horizon r_d.

- *Type-Ia supernovae (SN).* We exploit the `Pantheon+` sample of $\gtrsim 1500$ unique type-Ia SN in the redshift range $z \sim 0.01 - 2.3$ by [24] to fit for the magnitude-redshift relation $m_b = 5 \log[d_L(z)/\mathrm{Mpc}] + 25 + M_b$, where $d_L(z) = d_M\,(1+z)$ is the luminosity distance and M_b is the fiducial absolute magnitude of a type-Ia SN calibrated via the distance ladder (e.g., using Cepheids as an anchor).

- *Structure growth rate (SGR).* We exploit the sample of 18 robust and independent[5] measurements from different galaxy surveys in the redshift range $z \sim 0.02 - 1.4$ (see [107]) to fit for the structure growth rate $f\sigma_8(z) = \sigma_8\, |\mathrm{d}\delta_+/\mathrm{d}\ln a|$, where σ_8 is the rms amplitude of the perturbation spectrum on a scale of $8\,h^{-1}$ Mpc and δ_+ is the growing mode of the linear density contrast for the matter perturbations. The evolution of the latter quantity is computed by solving the differential equation (see appendix B)

$$\delta'' + (2 + H'/H)\,\delta' - (3/2)\,\Omega_m\,\delta = 0 \tag{3.2}$$

where the prime denotes differentiation with respect to $\ln a$; the adopted initial conditions are set at $\ln a_{\mathrm{ini}} \approx -3$ where $\delta_{\mathrm{ini}} = \delta'_{\mathrm{ini}} = a_{\mathrm{ini}}$ since we expect that at sufficiently high redshift (yet in the matter dominated epoch) the noise is negligible and thus $\delta = a$ applies as in the standard model.

---

[5]Correlations amongst the WiggleZ [14] data are taken into account, although they do not have a substantial impact in the final inference.

- *Cosmic chronometers (CC).* We exploit the sample of 33 measurements by [108] for the redshift-dependent Hubble rate $H(z)$ as determined from differential ages of early-type galaxies. We use the full covariance matrix, taking into account modeling uncertainties, mainly related to the choice of the initial mass function, of stellar libraries and stellar population synthesis models (see [109] for details).

For the analysis we adopt a Bayesian framework, characterized by the parameter set $\theta \equiv \{h_0, \Omega_{m,0}, \zeta, \alpha, r_d, M_b, \sigma_8\}$. We implement a Gaussian log-likelihood

$$\ln \mathcal{L}(\theta) = -\chi^2(\theta)/2\,, \tag{3.3}$$

where the chi-square $\chi^2(\theta) = \sum_{ij} \left[\mathcal{M}(\theta, z_i) - \mathcal{D}(z_i)\right] \mathcal{C}_{ij}^{-1} \left[\mathcal{M}(\theta, z_j) - \mathcal{D}(z_j)\right]$ is obtained by comparing our model expectations $\mathcal{M}(\theta, z_i)$ to the data values $\mathcal{D}(z_i)$, summing over different observables at their respective redshifts z_i and taking into account the variance-covariance matrix $\mathcal{C}_{ij}$ among redshift bins. We adopt flat priors $\pi(\theta)$ on the parameters $h_0 \in [0.5, 1.0]$, $\Omega_{m,0} \in [0, 1]$, $\zeta \in [0, 3]$ and $\alpha \in [-2, 0]$, $r_d\,[\mathrm{Mpc}] \in [120, 160]$, $M_b\,[\mathrm{mag}] \in [-20.5, -18.5]$, $\sigma_8 \in [0.6, 1.2]$. The bound $\Omega_{m,0} < 2/(4 - \alpha)$ is also set to ensure late-time physical solutions solving the cosmic coincidence problem (see section 2.4).

Moreover, when specified explicitly we add the following robustly accepted priors:

☐ *Horizon scale at drag epoch r_d.* We impose a prior on the horizon scale at the drag epoch. Since in ηCDM the pre-recombination physics is unaltered with respect to the standard cosmology (noise is negligible at high redshift) we rely on the ΛCDM value from [5] and adopt a Gaussian prior on r_d [Mpc] with mean 147.18 and dispersion 0.29.

☐ *Type-Ia SN zero-point magnitude.* We impose a prior[6] on the absolute magnitude M_b of a type-Ia SN derived from the distance ladder via Cepheids, variable asymptotic giant branch stars and the tip of the red giant branch. We adopt a Gaussian prior on M_b with mean -19.28 and dispersion 0.03, as suggested by [32] taking into account classic HST measurements and recent JWST cross-validation.

☐ *CMB first-peak angular scale.* We impose a prior on the angular scale of the first peak in the CMB temperature spectrum $\theta_\star \approx r_\star/d_M(z_\star)$, where $r_\star$ is the comoving sound horizon at recombination and $d_M(z_\star)$ is the transverse comoving distance at the recombination redshift $z_\star$. As above we assume a ΛCDM pre-recombination physics and thus set $r_\star \approx r_d/1.018$,[7] and $z_\star \approx 1090$ from [5]. Then we follow [13] and adopt a Gaussian prior on $100\,\theta_\star$ with mean 1.0411 and dispersion 0.0005, which is approximately twice the Planck [5] uncertainty.

---

[6]Note that the prior on M_b is correlated with the $z \lesssim 0.01$ SNe in the Pantheon+ dataset, which are thus excluded from the SN likelihood.

[7]The ratio $r_d/r_\star = 1.01841 \pm 0.00033$ of the sound horizon at last scattering ($r_\star$) and at the drag epoch (r_d) is completely correlated with the baryon density $\Omega_b\,h^2 = 0.02237 \pm 0.00015$ [5]. By adopting a fixed value for $r_d/r_\star$ implies we are setting the baryon contribution to the total matter density, which is the only free parameter. Note that we also neglect the overall correlation between $\theta_\star$ and r_d when imposing both priors; actually the mild correlation between these parameters (with a coefficient ~ 0.17) has no major impact on our final inference outcomes.

Dataset(s)	h_0	$\Omega_{m,0}$	ζ	α	r_d [Mpc]	$-M_b$ [mag]	σ_8
BAO^{r_d}	$0.68^{+0.02}_{-0.02}$	$0.39^{+0.04}_{-0.03}$	$1.37^{+0.11}_{-0.11}$	$-0.89^{+0.37}_{-0.26}$	$147.2^{+0.3}_{-0.3}$	–	–
$\text{BAO}^{r_d}+\text{SN}^{M_b}$	$0.69^{+0.01}_{-0.01}$	$0.40^{+0.03}_{-0.02}$	$1.44^{+0.04}_{-0.04}$	$-0.69^{+0.19}_{-0.12}$	$147.1^{+0.3}_{-0.3}$	$19.38^{+0.02}_{-0.02}$	–
$\text{BAO}^{r_d}+\text{SN}^{M_b}+\text{SGR}^{\theta_\star}+\text{CC}^{t_0}$	$0.69^{+0.01}_{-0.01}$	$0.41^{+0.01}_{-0.01}$	$1.46^{+0.04}_{-0.03}$	$-0.77^{+0.08}_{-0.06}$	$147.1^{+0.3}_{-0.3}$	$19.38^{+0.02}_{-0.02}$	$0.78^{+0.03}_{-0.03}$
SN^{M_b}	$0.72^{+0.01}_{-0.01}$	$0.26^{+0.09}_{-0.09}$	$1.60^{+0.15}_{-0.23}$	$-0.90^{+0.77}_{-0.39}$	–	$19.28^{+0.03}_{-0.03}$	–
$\text{BAO}+\text{SN}+\text{SGR}^{\theta_\star}+\text{CC}^{t_0}$	$0.68^{+0.02}_{-0.02}$	$0.40^{+0.03}_{-0.01}$	$1.36^{+0.07}_{-0.07}$	$-0.87^{+0.15}_{-0.10}$	$147.6^{+2.6}_{-2.6}$	$19.40^{+0.04}_{-0.04}$	$0.78^{+0.05}_{-0.05}$

Table 1. Marginalized posterior estimates (mean and 1σ confidence intervals are reported) from the MCMC analysis of different cosmological datasets with the ηCDM model. Columns report the values of the (normalized) Hubble constant h_0, present matter density $\Omega_{m,0}$, noise parameters ζ and α, horizon scale at drag epoch r_d, SN Ia absolute magnitude M_b, and amplitude of linear matter perturbation spectrum σ_8. The rows refer to the different dataset combinations exploited for the fit: first line is for BAO with the prior on r_d; second line adds SN with the prior on M_b; third line adds SGR and CC with the priors on $\theta_\star$ and t_0; forth line is for only SN with the prior on M_b, and last line is for the combined datasets (as in the third line) but with no priors on r_d and M_b.

☐ *Age of the Universe.* We impose a prior on the age of the Universe from globular cluster dating. We adopt a Gaussian prior on t_0 [Gyr] with mean 13.5 and dispersion 0.4 as suggested from [110].

We sample the parameter posterior distributions $\mathcal{P}(\theta) \propto \mathcal{L}(\theta)\,\pi(\theta)$ via the MCMC Python package `emcee` [111], running it with 10^5 steps and 100 walkers; each walker is initialized with a random position extracted from the priors discussed above. To speed up convergence, we adopt a mixture of differential evolution and snooker moves of the walkers, in proportion of 0.8 and 0.2 respectively, that emulates a parallel tempering algorithm. After checking the auto-correlation time, we remove the first 30% of the flattened chain to ensure burn-in.

3.2 Results

The results of our Bayesian analysis are displayed in figure 2 and reported in table 1. Specifically, in figure 2 we illustrate the MCMC posterior distributions on the fitting parameters for various datasets (color-coded); the marginalized distributions are normalized to unity at their maximum, and the crosses mark the best-fit values of the parameters for the joint analysis. In table 1 we summarize the marginalized posterior estimates of the parameters (median values and 1σ credible intervals).

We first analysed separately BAO data with the prior on r_d from CMB (first line in table 1) and SN data with the prior on M_b from the cosmic ladder (fourth line in table 1). From BAO we find rather well constrained values of $h_0 \approx 0.68$ and $\Omega_m \approx 0.4$ and noise strength $\zeta \approx 1.4$, while the noise evolution parameter $\alpha \approx -0.9$ is loosely estimated. From SN we find a Hubble constant $h_0 \approx 0.72$ (which reflects the prior on M_b) higher than BAO and a matter density $\Omega_{m,0} \approx 0.3$ lower than BAO though not particularly well constrained, a noise strength $\zeta \approx 1.6$ slightly larger than BAO, and no robust inference on the noise
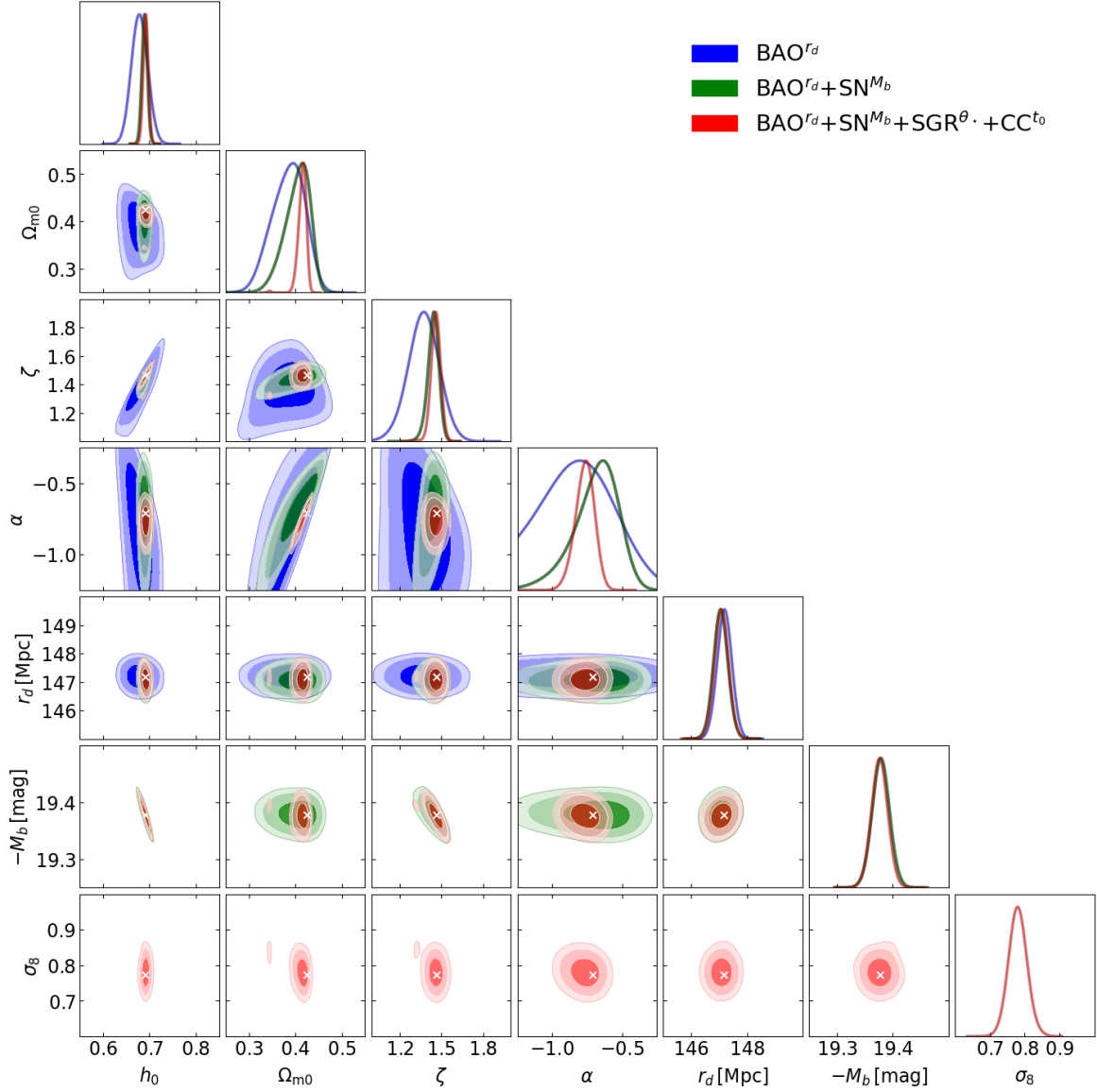
Figure 2. MCMC posterior distributions of the (normalized) Hubble constant h_0, present matter density parameter $\Omega_{m,0}$, noise parameters ζ and α, horizon at the drag epoch r_d, type-Ia SN zero-point magnitude M_b and amplitude of the linear matter power spectrum σ_8. Coloured contours/lines refer to the analysis with different dataset(s): blue is for BAO with the prior on r_d; green adds SN with the prior on M_b; red adds SGR and CC with the priors on $\theta_\star$ and t_0. The marginalized distributions are in arbitrary units (normalized to 1 at their maximum value). The white crosses highlights the position of the best fit values for the full dataset.
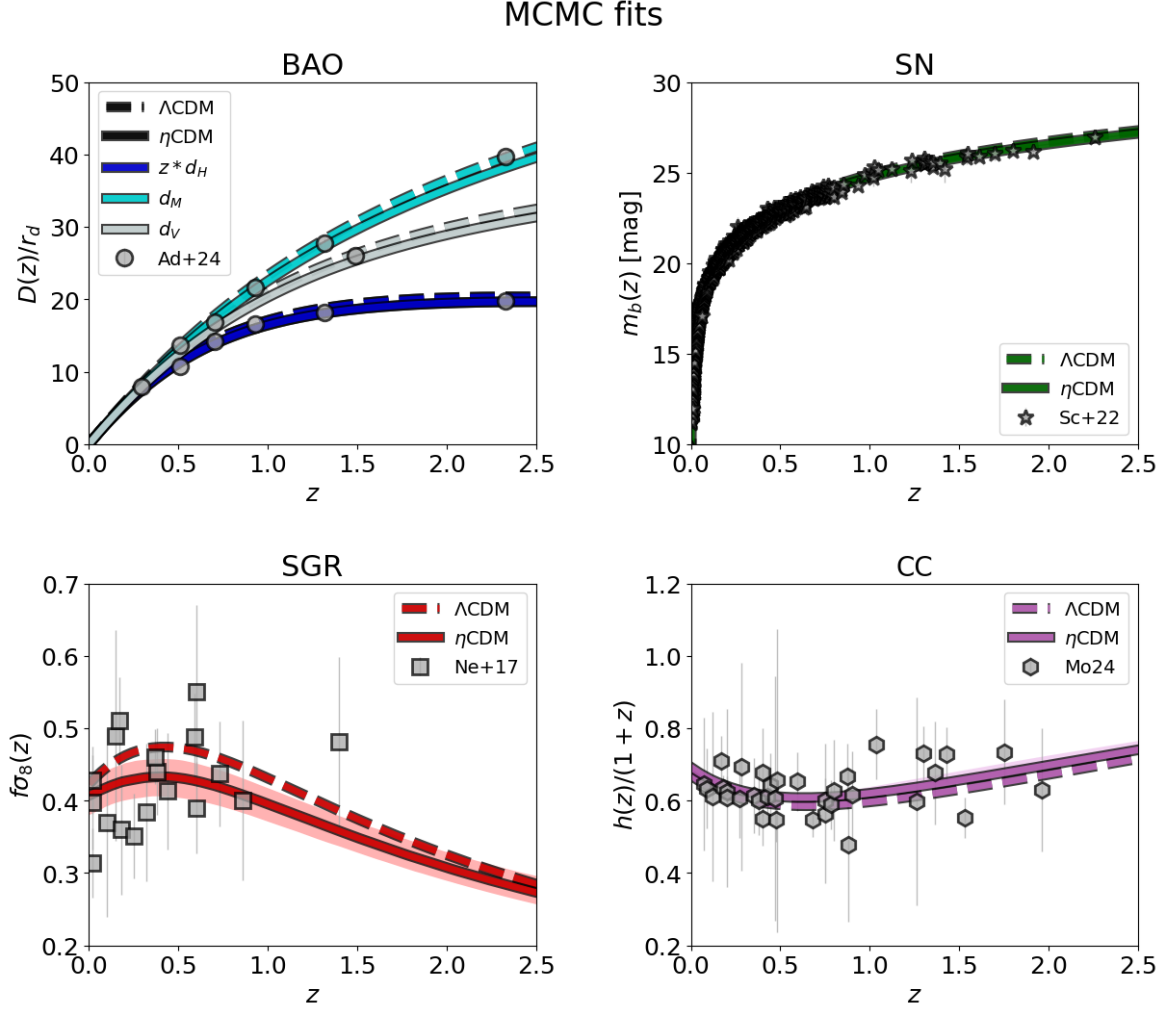
Figure 3. MCMC fits to the BAO distance ratios (top left panel) $d_H(z)/r_d$ (blue) $d_M(z)/r_d$ (cyan) $d_V(z)/r_d$ (azure), type-Ia SN magnitude vs. redshift $m_b(z)$ (top right), structure growth rate $f\sigma_8(z)$, cosmic chronometer determination of the (normalized) Hubble rate $h(z)$ in the ηCDM model. Colored lines illustrate the median, and the shaded areas show the 2σ credible interval from sampling the posterior distributions. For reference, the dashed lines display the standard ΛCDM model with parameter set from `Planck` [5]. Data are from [13] (circles), [24] (stars), [107] (squares), and [108] (hexagons).

evolution parameter α. However, all the parameters (and in particular h_0) from the BAO and SN analyses are consistent within $\sim 1.5\sigma$, so that no statistically-significant Hubble tension exists in ηCDM.

Provided that, we combine the BAO and SN datasets to improve our constraining power, especially in relation to the noise parameters (second line in table 1). In fact, both the noise strength $\zeta \approx 1.44$ and the noise evolution $\alpha \approx -0.7$ are considerably better constrained, though the latter retains a quite appreciable uncertainty. The Hubble constant moves to $h_0 \approx 0.7$, with the related value of r_d staying put with respect to the prior from CMB, while the type-Ia SN zero-point M_b is shifted from the mean prior value of $\lesssim 2\sigma$.

Finally, we perform a joint analysis by adding the structure growth rate and cosmic chronometers data, with priors on the CMB $\theta_\star$ and on the age of the Universe t_0 from globular cluster dating (third line in table 1). This allows us to refine considerably the determination of the noise evolution parameter $\alpha \approx -0.8$, and to obtain a rather precise estimate for the normalization of the linear matter power spectrum $\sigma_8 \approx 0.78$. The latter is found to be soundly consistent with the CMB expectation around 0.81, so that no $f\sigma_8$ tension exists in the ηCDM model. No strong degeneracies among the parameters emerge, apart from low-degree dependencies among h_0 vs. ζ vs. M_b, and between $\Omega_{m,0}$ vs. α.

We repeat this joint analysis of the overall datasets without imposing priors on r_d and M_b, to test whether these could bias significantly some of our inferences (last line in table 1). This is not the case, as all the parameters are found to be consistent with the priorized analysis within $\lesssim 1\sigma$; moreover, the uncertainties on all model parameters are marginally enlarged. Interestingly, the SN zero-point is very well constrained also in this case, while the r_d determination has a substantially larger uncertainty. In addition, the value of h_0 which is now mainly guided by the CC data instead of the inverse-distance ladder (prior on r_d is not assumed) is identical to the constraints imposed by the latter, indicating a high degree of consistency amongst datasets within the ηCDM model.

Comparing with the previous joint analysis in [1], the bestfit parameters found in this work, despite being consistent within 2σ, show a few appreciable differences. The most noticeable ones were generally higher values $h_0 \gtrsim 0.7$ and smaller values of $\alpha \lesssim -1$ found there. We have tested that such differences are driven by two reasons. The first is the much precise BAO datasets employed in the present analysis. Specifically, here we fit for the BAO distance scale ratios d_M/r_d, d_H/r_d and d_V/r_d while in [1] only spherically-averaged BAO data were considered. The second is the revised prior on M_b, that in turn strongly determines the value of and uncertainty on h_0 from SN. In [1] the extremely stringent prior from the Cepheid anchor by [31] was employed, while here we adopt the more balanced one from [32] that overall yields a lower h_0 with a slightly larger uncertainty. The combination of these two occurrences in [1] weighted low the BAO data and high the SN ones in the joint analysis, driving the bestfit toward a higher value of h_0 and a smaller (and more uncertain) value of α.

We stress the relevance of the SGR data considered in this work, which provide quite stronger constraint on α with respect to the BAO+SN combination alone. This is because α determines the redshift evolution of the noise, and in turn considerably affects the overall behavior of the Hubble parameter and of the growth factor in the redshift range probed by galaxy redshift surveys. In principle, further constraints on the noise parameters ζ and α can be provided by BAO-independent determinations of the Hubble rate such as those offered by cosmic chronometers. We include such data in our analysis, but their present uncertainties are so large that they marginally contribute to the overall parameter inference. The situation, hopefully, will improve in the near future with new datasets from galaxy surveys and a better control on systematics uncertainties related to stellar and galaxy evolution models in cosmic chronometer measurements (see [108] for an extended discussion).

In figure 3 the best fits (solid lines) and the 2σ credible intervals (shaded areas, in most cases barely visible because they are very narrow) sampled from the posteriors are projected onto the observables: BAO distance ratios, type-Ia SN magnitude vs. redshift
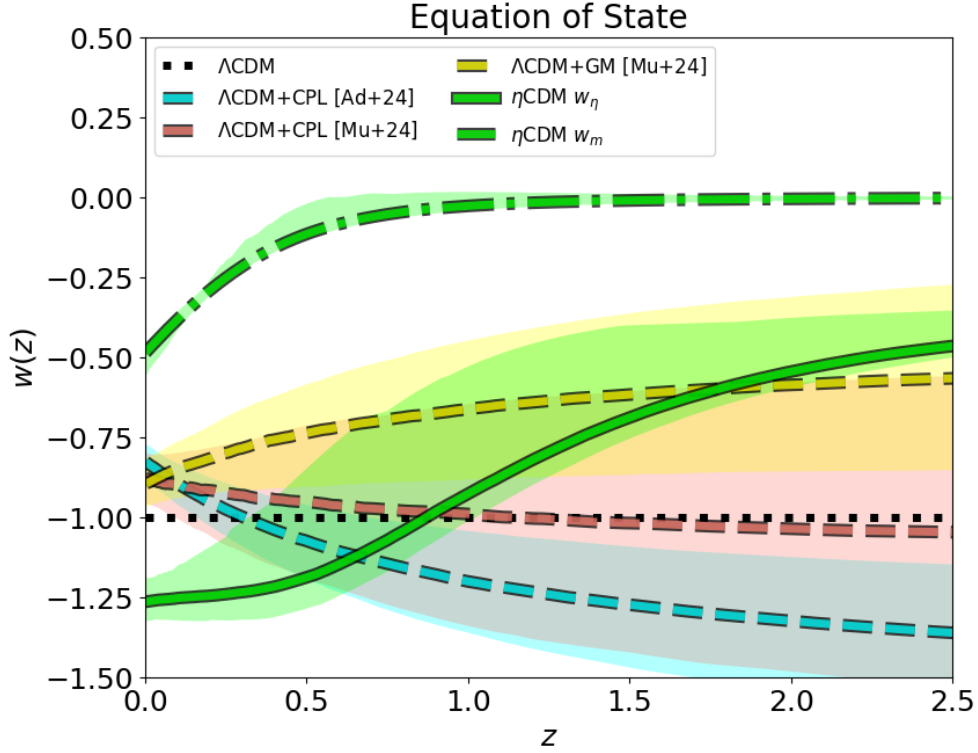
Figure 4. Evolution of the equation of state. Green is the result for the ηCDM model from our analysis (solid for emergent dark energy w_η and dot-dashed for matter w_m). Cyan is the result w_Λ from the ΛCDM+CPL analysis of BAO+SN data by [13], red from the ΛCDM+CPL analysis of BAO+SN+SGR data by [112] and yellow from a ΛCDM+generalized CPL analysis of BAO+SN+SGR data by [112]. For reference, dotted black line is the value $w_\Lambda = -1$ of the standard ΛCDM model.

diagram, structure growth rate $f\sigma_8(z)$, and Hubble rate $h(z)$ to be confronted with cosmic chronometers. The fits are always extremely good, with overall reduced $\chi_r^2 \lesssim 1$. For reference, the outcomes on the same observables for the standard ΛCDM model with parameter set from `Planck` [5] are also reported. All in all, the performances of the ηCDM and ΛCDM model are very similar; this is also confirmed by Bayesian comparison testing in terms of the Bayesian evidence or of Bayes inference criterion, that as expected do not show any reasonable preference in favor of either models. Maybe the most relevance difference is in the evolution of the $f\sigma_8$ parameter with redshift, a potentially interesting probe that we will discuss more deeply in section 4.2.

4 Discussion

In this section we focus on, and discuss some relevant consequences of the above analysis.

4.1 Dark energy equation of state

In figure 4 we show in green the equation of state for the emergent dark energy component in the ηCDM model. Solid line is the median and shaded area is the 1σ confidence intervals from sampling the posterior distributions from our MCMC analysis of joint cosmological

datasets. As anticipated already in section 2 the dark energy equation of state parameter w_η has a decreasing trend from values close to $w_\eta \approx -1/3$ at high redshift down to values $w_\eta \lesssim -1$ at the present time (and then coming back asymptotically to $w_\eta \to -1$ in the infinite future). First of all, we stress that in the ηCDM model one should not be strongly concerned by values of $w_\eta < -1$. In fact, while for a dynamical dark energy field these values would imply a violation of the null energy condition, in the ηCDM model dark energy is just a description for the accelerated expansion of the Universe, emergent from the noise associated to structure formation.

The same is true for the matter component (reported as a green dot-dashed line in figure 4), whose equation of state is apparently modified from $w_m \approx 0$ at high redshift to values $w_m \lesssim -0.5$ at the present time (and toward $w_m \to -1$ in the infinite future). In fact, the properties of cold DM particles are clearly not affected by the noise associated to structure formation. What changes is the evolution of $\rho_m(z) = \Omega_m h^2$ with redshift, in such a way of originating an apparent decrease in $w(z)$ if one insists in describing the ensemble-averaged matter density with the standard fluid mass-energy conservation equation.[8] As anticipated, such a behavior is often present in cosmological models with a strong-coupling in the dark sector (e.g., [95–97, 113]), to which the ensemble-averaged ηCDM evolution is similar, because dark energy is emergent from structure formation hence it depends on matter density.

Coming back to $w_\eta(z)$, our results could be compared with a few recent studies where the dark energy parameter w_Λ of the ΛCDM model has been reconstructed from minimal extensions of such a basic framework. In particular, [13] have adopted the standard CPL [114, 115] parametrization $w_\Lambda(a) = w_0 + w_a (1-a)$ in terms of the scale factor a and fitted BAO+SN data for (w_0, w_a). The result is reported in figure 4 as a cyan line and tends to imply a dark energy strongly decreasing toward the past, so violating the null energy condition for $z \gtrsim 0.5$. The same analysis based on the CPL parametrization has been refined by [112] by fitting BAO+SN+SGR data. Their outcome is shown in red, and implies a w_Λ mildly decreasing from the present values toward the past, with $w_\Lambda \approx -1$ at $z \gtrsim 1$. Finally, the same authors [112] have also fitted the BAO+SN+SGR data with a parametrized modification of the expansion history inspired by modified gravity theories, and derived the constraints on $w_\Lambda(z)$ reported in yellow. Their results suggest a $w_\Lambda(z)$ increasing with redshift, with an overall behavior qualitatively similar to the ηCDM model. This is not surprising, since their parametrization can empirically describe interacting dark energy models [see for instance 98], which formally may resemble ηCDM.

All in all, these estimates concerning $w_\Lambda(z)$ are considerably uncertain and critically dependent on the adopted empirical parametrization of the dark energy equation of state and/or of the expansion history, so drawing any strong conclusions is premature. However, the take-home message from the ηCDM model is that the equation of state parameter for the dark energy may be not so fundamental, in that it could just reflect a modified evolution in the expansion history due to an emergent phenomenon.

---

[8]Basically one is imposing the separate conservation of the stress energy tensor for each fluid component, while this is not the case at late times since matter and emergent dark energy are coupled. Plainly conservation of DM particles' number is not affected.
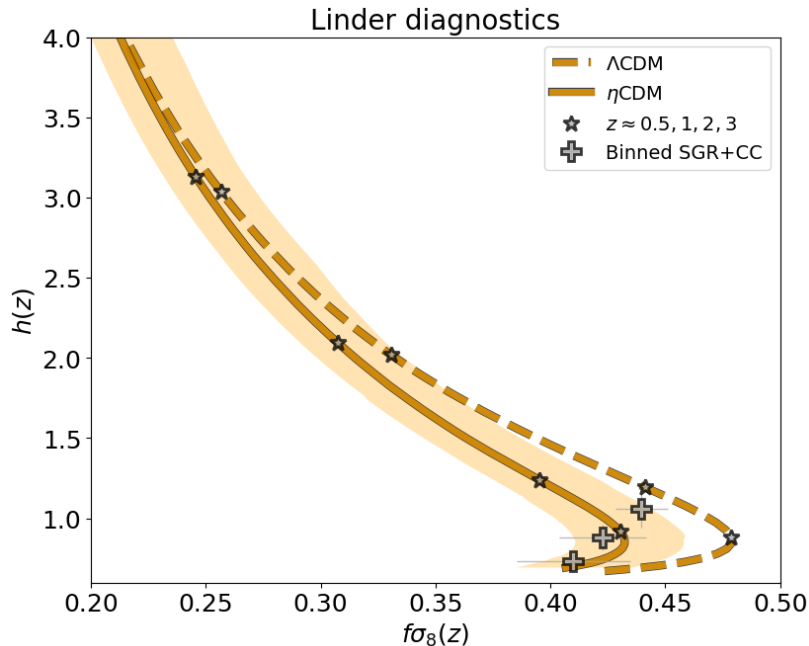
Figure 5. Linder's diagnostic plot of the Hubble rate vs. the structure growth rate. Orange is the result for the ηCDM model from our analysis (solid line is the mean and shaded area is the 1σ confidence interval). Dashed line refers to the standard ΛCDM model with parameter set from `Planck` [5]. Stars on both the solid and dashed lines highlight the location of the redshifts $z \approx 0.5$, 1, 2 and 3 along the curves from bottom to top. The plus symbols show the CC [108] and SGR [107] data binned in common redshift intervals $z < 0.2$, $0.2 < z < 0.6$, and $0.6 < z < 1.2$ that contain almost the same number of SGR data points.

4.2 Linder's diagnostic as a crucial probe of ηCDM?

As mentioned in section 1 it is not easy to identify an observational probe that can clearly distinguish ΛCDM from any alternative model. This is because, admittedly, the standard scenario fits remarkably well to the cosmological data over a very extended range of spatial and temporal scales, so that any reasonable alternative model should have very similar phenomenological outcomes. Here we propose that a specifically designed observable to test the ηCDM model and possibly to allow selecting or rejecting it against the ΛCDM framework is constituted by the Linder's diagnostics [116]. The latter is just a plot of the conjoined background expansion and structure growth rates $H(z)$ vs. $f\sigma_8(z)$, as illustrated in figure 5.

The result for the ηCDM model from our analysis is reported as a solid line with shaded area (median and 1σ confidence intervals), and compared with the expectation from ΛCDM [5] in yellow dashed. For both models, stars highlight the location of redshifts $z \approx 0$, 1, 2, 3 along the curves from bottom to top. Differences between the two models are negligible at high z while they progressively develop toward lower redshift where the effects of the noise associated to structure formation kicks in. In particular, the ηCDM model features a less prominent bump or wiggle at $z \lesssim 0.5 - 1$. We also report as plus symbols the $f\sigma_8(z)$ data from galaxy surveys [107] and $h(z)$ measurements from cosmic chronometers [108], binned in redshift intervals which contain an almost equal numbers of the former data points (which
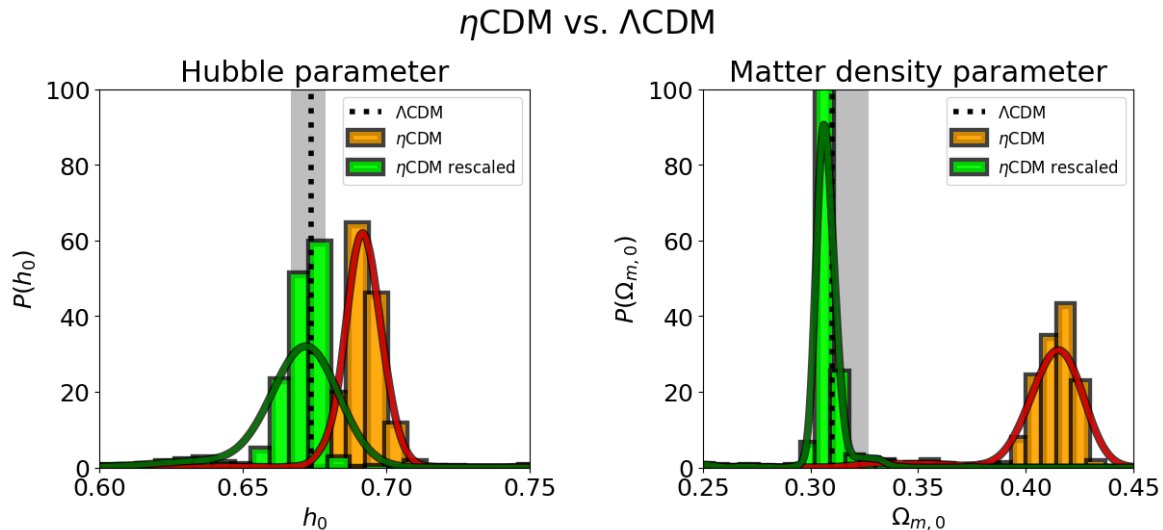
Figure 6. Posterior probability distributions on the Hubble constant h_0 (left panel) and on the matter density parameter $\Omega_{m,0}$ (right panel) from our analysis of cosmological data with the ηCDM model. The orange histograms refer to the values at the present time in ηCDM, while the green ones to that measured at the recombination epoch in ηCDM and then scaled to the present according to the ΛCDM evolution; this is done for a fair comparison with the ΛCDM results based on `Planck` CMB data [5], which are illustrated by the dotted lines with grey shaded area (median and 1σ confidence intervals). The solid lines display Gaussian density kernel estimates to the histograms.

are less numerous and extend to appreciably lower z). We stress that the error bars are just the variance on the stacked mean but do not reflect systematic uncertainties, especially for cosmic chronometers data.

Overall the ηCDM model reproduces very well the binned data, while the ΛCDM would require σ_8 to be appreciably lower than the value ≈ 0.81 expected from CMB. The latter is a manifestation of the well-known $f\sigma_8$ tension suffered by standard ΛCDM model [107], which is instead absent in our ηCDM framework. Apart from this general statement, we caveat that uncertainties are still too large and the redshift coverage too narrow in the data to draw definite conclusions. However, future galaxy survey more precisely pinpointing the $f\sigma_8$ parameter in the redshift range $z \lesssim 1$, and more robust determinations of the Hubble rate by cosmology-independent methods such as cosmic chronometers will be extremely relevant and could possibly allow a robust model selection according to this diagnostic plot.

Note that other interesting diagnostic could be possibly constituted by redshift drift measurements or a combination of these with cosmic chronometers, as proposed by [117]. However, the Linder's test discussed above has the huge advantage that it can be promptly exploited with current or upcoming data, while precise redshift drift measurements will plausibly require decades to be collected.

4.3 ηCDM vs. ΛCDM: Hubble rate and matter density

In figure 6 we illustrate in orange the marginalized posterior distributions of the Hubble constant h_0 and the matter density $\Omega_{m,0}$ in the ηCDM model from our analysis. Specifically,

the histograms refers to the binned MCMC chains while the solid lines is a Gaussian kernel density estimate to them.

One may be concerned that with appreciably high values of the Hubble constant $h_0 \approx 0.7$ and above all of the matter density $\Omega_{m,0} \approx 0.4$ in ηCDM there could be problems with reproducing the overall CMB spectrum. However, these values could be misleading, since the evolution of $h(z)$ and $\Omega_m(z)$ in the ηCDM model considerably differ from the standard ΛCDM scenario after recombination during the era of structure growth (see figure 1). What is really important to reproduce the CMB spectrum are not the values at the present, but those at the recombination epoch $z_\star \approx 1100$. To check that the ηCDM model is safe in this respect, we computed $h(z_\star)$ and $\Omega_m(z_\star)$ in ηCDM, and then (just because it is customary to report the values at present time), we evolve them back to the present according to the ΛCDM model. Note that in evolving h and Ω_m to the recombination redshift in ηCDM we have taken into account the full MCMC chains, hence the correlations between cosmological and noise parameters. In particular, the degeneracy among h vs. Ω_m vs. α causes the dispersion in $h(z_\star)$ to be slightly larger than that in h_0 and the dispersion in $\Omega_m(z_\star)$ to be appreciably smaller than that in $\Omega_{m,0}$.

The net results are the green histograms and lines (referred in the caption as ηCDM rescaled), that can be directly compared with the bestfit ΛCDM values from `Planck` [5] reported in the figure as dotted lines with grey shaded areas (median and 1σ confidence interval). In other words, if the green histograms and the dotted line agree, it means that the recombination values of the Hubble rate h and matter density Ω_m (hence also the physical density $\rho_m \propto \Omega_m\, h^2$) in ηCDM and ΛCDM are consistent. This is indeed the case, testifying that no big issue with the full CMB power spectrum is expected. A full analysis of the latter in the ηCDM framework will be pursued in the next future.

The argument can be reversed to better understand why in ηCDM a value of $\Omega_{m,0} \approx 0.4$ higher than in ΛCDM is found. In fact, we have seen that the matter component in the ηCDM model features a non-trivial equation of state, decreasing from values $w_m \approx 0$ at early times to $w_m < 0$ at late times. This means that the dilution of matter by the expansion $\rho_m \propto a^{-3\,(1+w_m)}$ is reduced relative to the standard scenario that has $w_m = 0$ hence $\rho_m \propto a^{-3}$ at any epoch. Therefore starting from similar values of Ω_m at the recombination epoch required to fit CMB data, it is somewhat expected that at present $\Omega_{m,0}$ should be higher in ηCDM than in ΛCDM.

4.4 Broad comparison with other cosmological datasets

In figure 7 we illustrate as colored shaded areas ($1-2\sigma$ confidence intervals) the constraints in the σ_8 vs. $\Omega_{m,0}$ and $S_8 \equiv \sigma_8\,(\Omega_{m,0}/0.3)^{1/2}$ vs. $\Omega_{m,0}$ planes from various cosmological probes not employed in this work: cosmic shear measurements from `DES` [119] and `KiDS` [118], full CMB temperature and polarization spectra from `Planck` [5], and cluster statistics from `eROSITA` [22]. All these constraints have been inferred in the standard ΛCDM scenario and have been shown to stay put in minimal extensions of it. From the diagrams one can clearly spot the so called S_8 tension of the ΛCDM model, in that the cosmic shear measurements tend to prefer appreciably lower values of S_8 with respect to CMB and cluster statistics.
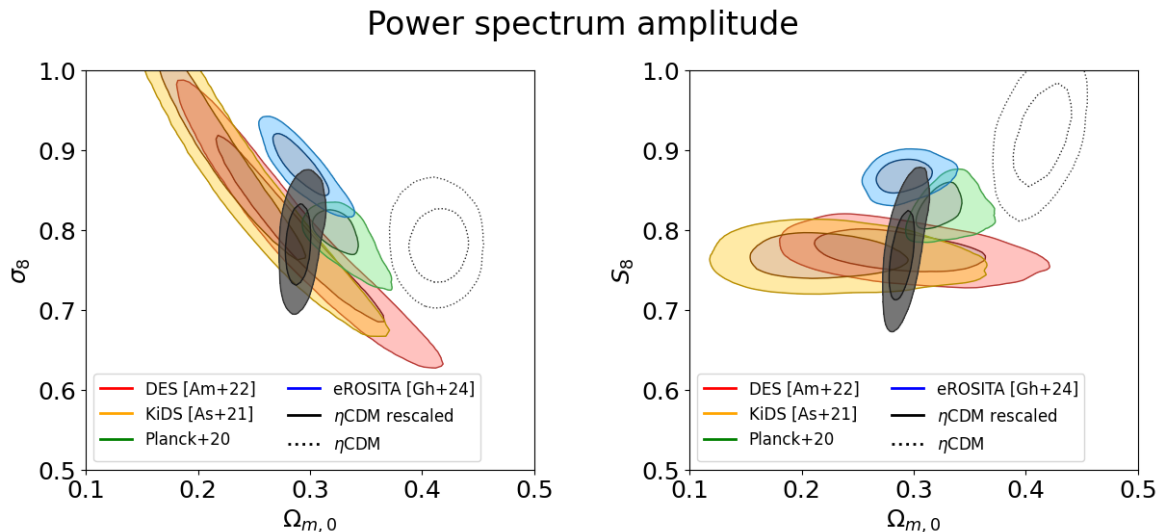
Power spectrum amplitude

Figure 7. Constraints on the linear matter power spectrum amplitude in terms of the parameter σ_8 (left panel) or $S_8 \equiv \sigma_8\,(\Omega_{m,0}/0.3)^{1/2}$ (right panel) vs. the matter density $\Omega_{m,0}$. Colored contours report the $1\sigma - 2\sigma$ confidence intervals from cosmic shear measurements by `KiDS` [118] (orange) and `DES` [119] (red), from cluster statistics by `eROSITA` [22] (blue), from CMB by `Planck` [5] (green), and from our analysis with the ηCDM model (black) when $\Omega_{m,0}$ has been rescaled from the recombination value to the present with the ΛCDM evolution for fair comparison (for reference, the dotted contours refers to the present values in ηCDM).

The outcomes of the ηCDM model from our joint analysis of BAO+SN+SGR+CC data are reported as a grey shaded area. Here $\Omega_{m,0}$ has been rescaled to the present time as discussed in the previous section, to allow for a fair comparison with the constraints from the other cosmological datasets that are based on the ΛCDM model (the face value contours of ηCDM would be given by the dotted lines). There is an overall good agreement of the ηCDM constraints from this work with the other datasets reported in figure 7. We stress, however, that a full fitting of cosmic shear data, CMB power spectra in temperature and polarization and cluster mass function with the ηCDM model would be required to quantitatively confirm this broad agreement. This is non-trivial and goes beyond the scope of the present paper, hence it will be pursued in forthcoming works.

5 Summary and conclusions

The ηCDM is a new cosmological model by [1] aimed to cure at once some drawbacks of the standard ΛCDM scenario, such as the violation of the cosmological principle at late-times due to structure formation, the origin of the cosmic acceleration, and the cosmic tensions. To this purpose, the model adopts a statistical perspective envisaging a stochastic evolution of large-scale patches in the Universe with typical sizes $10 - 50\,h^{-1}$ Mpc, which is meant to describe the complex gravitational processes leading to the formation of the cosmic web. The stochasticity among different patches is technically rendered via the diverse realizations of a multiplicative noise term ('a little ado') in the cosmological equations, and the overall background evolution of the Universe is then operationally defined as an average over the

patch ensemble (see section 2.1). In [1] we have shown that in ηCDM model an accelerated expansion is naturally obtained at late cosmic time without the need for any postulated dark energy component, since as structure formation proceeds in the Universe an increasing amount of its volume is statistically occupied by low-density regions (i.e., voids) featuring an enhanced expansion rate.

In this work we have provided new theoretical perspectives on the ηCDM model, and we have performed further observational tests against the most recent cosmological datasets. Specifically, our main findings are as follows:

- We have shown that the ensemble-averaged evolution of the Universe in ηCDM can be rendered in terms of a spatially flat cosmology and of an emergent dark energy component with a time-dependent equation of state (see section 2.2), originating the present cosmic acceleration. The effects of the noise can be viewed as transforming a curvature-like term in the early Universe into an emergent dark energy at late times. For the mechanism to work it is required that the ensemble-averaged spatial curvature in the early Universe is negative, albeit it can be arbitrarily small.

- We have highlighted that in ηCDM also the matter density features a non-standard evolution at late times, that may be described in terms of a progressively decreasing equation of state parameter $w_m < 0$. Such a behavior often occurs in models with strong coupling in the dark sector, as ηCDM to some extent is: dark energy emerges from structure formation hence depends on the evolution of the matter content, which is in turn affected by the late-time acceleration induced by the emergent dark energy (see section 2.2).

- We have provided handy expressions for the cosmographic parameters of the ηCDM model, suitable for a quick implementation in the analysis of future datasets (see section 2.3).

- We have shown that no coincidence issue is present in the ηCDM model, since at variance with the standard scenario the ensemble-averaged values of the cosmological quantities will stay very close to the present one for a infinite amount of time in the future (see section 2.4).

- We have compared the ensemble-averaged evolution of the ηCDM framework to the reference ΛCDM model, finding that they feature very similar behaviors in terms if the expansion rates, cosmological timescales, cosmographic parameters, distance scales, energy densities, etc. (see section 2.5 and figure 1). The most relevant differences can be spotted in the evolution of the energy density parameters of the matter and of the emergent dark energy (and correspondingly in their equations of state) and in the runs of the jerk and snap parameters at intermediate to high redshift. These could be possibly tested with `Euclid` via weak lensing and clustering analysis, and with future surveys like those planned on the `Nancy Grace Roman Space Telescope` via searches for transient objects (e.g., SNe).

- We have tested the ηCDM model against the most recent SN Ia, BAO and structure growth rate datasets (including the `Pantheon+` and `DESI` latest releases) via a standard

Bayesian analysis framework (see section 3.1), finding a very good agreement (see section 3.2, figures 2–3 and table 1).

- We have demonstrated that in ηCDM both the H_0 and the $f\sigma_8$ tensions are substantially alleviated, if not solved at all (see section 3.2, figure 2 and table 1). Specifically, the H_0 tension is alleviated since, adopting an inverse ladder approach (which is natural since ηCDM is indistinguishable from ΛCDM at high redshift when structure formation is still in its early and linear stages), values of $h_0 \approx 0.7$ could decently fit both BAO and type-Ia SN data. Moreover, the $f\sigma_8$ tension is solved since the growth factor of the ηCDM model has a different evolution and allows to fit the structure growth rate data with an appreciably higher $\sigma_8 \approx 0.8$ than in ΛCDM, so as to be consistent with CMB expectations.

- We have discussed the evolution of the equation of state for the emergent dark energy, that starts from curvature-like values $w_\eta \approx -1/3$ at early times and decreases toward $w_\eta \lesssim -1$ at late times so enforcing an accelerated expansion. We have also compared our findings to various CPL parameterization adopted in recent analysis of cosmological data with the ΛCDM model, though the large uncertainties in the reconstruction preclude any robust conclusion (see section 4.1 and figure 4).

- We have stressed that the Linder's diagnostic plot of the redshift-dependent Hubble parameter $H(z)$ vs. structure growth rate $f\sigma_8(z)$ could be a powerful probe of the ηCDM model in the near future (see section 4.2 and figure 5). Precise estimates of the $f\sigma_8$ parameter in the redshift range $z \lesssim 1$ by upcoming galaxy surveys, and robust determination of the redshift-dependent Hubble rate by cosmology-independent methods such as cosmic chronometers will be extremely relevant for quantitatively contrasting and distinguishing the ηCDM model against the standard scenario.

- Although the ηCDM model requires a present matter density and Hubble parameters $\Omega_{m,0} \approx 0.4$ and $h_0 \approx 0.7$ higher than in the standard scenario (based on CMB and BAO data), we have pointed out that the corresponding values of $\Omega_m(z)$ and $h(z)$ at high-redshift agree with those in ΛCDM, thus ensuring broad consistency with CMB power spectra, cosmic shear surveys and galaxy cluster statistics (see section 4.4 and figures 6 and 7). An in-depth analysis of these datasets is however non-trivial and deferred to future works.

As a concluding remark, we would like to stress that the foundational hypothesis (i.e., a stochastic perspective in place of the deterministic view based on the canonical cosmological principle) and the main outcome (i.e., dark energy as an emergent phenomenon instead of a cosmological constant or dynamical field) of this work could be anyway helpful for future studies aimed at revisiting the standard cosmological framework, independently of the details in the specific model considered here. As to the stochastic perspective, could it be useful to address some further 'anomalies' of the standard framework (e.g., [91]) like those related to considerable cosmic bulk flows on large scales (see [41, 49]) and/or to the presence of supergiant structures in the Universe (see [120–122])? As to the emergent dark energy, could one relate it to some form of gravitational energy associated to virialized

structures/voids or geometric curvature (e.g., [73, 123, 124])? All these would constitute extremely relevant questions to be addressed in the near future for paving the way toward an improved model of physical cosmology.

Acknowledgments

A ηCDM and cosmological spatial averaging

In this appendix we review the issue of spatial averaging in Newtonian cosmology, as developed by many literature studies focused on deterministic backreaction (e.g., [66, 67]), to establish a connection with the ηCDM model. Specifically, we aim to clarify the origin, and quantitatively assess the scale-dependent strength of the stochasticity in the mass-energy conservation equation that is at the heart of the ηCDM framework.

Our discussion is based on the well-known assumptions that the large-scale dynamics of the Universe can be approximately described in Newtonian gravity (as adopted in cosmological numerical simulations; e.g., for a review see [125]), and that the evolution of the various matter and energy components can be treated in the fluid approximation. In this vein, we start by writing the continuity, Euler and Poisson equation for a (pressureless) cosmological fluid with density field $\rho(\mathbf{r}, t)$ and velocity field $\mathbf{u}(\mathbf{r}, t)$ as:

$$\begin{cases} \partial_t \, \rho + \nabla_{\mathbf{r}} \left(\rho \, \mathbf{u} \right) = 0 \, , \\ \partial_t \, \mathbf{u} + \left(\mathbf{u} \cdot \nabla_{\mathbf{r}} \right) \mathbf{u} = -\nabla_{\mathbf{r}} \, \phi \, , \\ \nabla_{\mathbf{r}}^2 \, \phi = 4\pi G \, \rho \, . \end{cases} \tag{A.1}$$

We switch to the comoving coordinate $\mathbf{x}$ defined via $\mathbf{r} = a(t) \, \mathbf{x}$, with $a(t)$ being the scale factor. We obtain $\mathbf{u} = \dot{\mathbf{r}} = \dot{a} \, \mathbf{x} + a \, \dot{\mathbf{x}}$, where the last addendum is just the peculiar velocity.

In the new coordinates $\nabla_{\mathbf{r}} = (1/a)\,\nabla_{\mathbf{x}}$ and $\partial_t|_{\mathbf{r}=\text{const.}} = \partial_t|_{\mathbf{x}=\text{const.}} - H\,(\mathbf{x}\cdot\nabla_{\mathbf{x}})$ hold, with $H \equiv \dot{a}/a$ representing the expansion rate. The continuity equation can be rewritten as

$$\dot{\rho} + 3H\,\rho = -\rho\,\theta\,, \tag{A.2}$$

where we have defined the comoving peculiar velocity divergence field $\theta \equiv \nabla_{\mathbf{x}}\cdot\dot{\mathbf{x}}$ and the total derivative along the fluid flow $\mathrm{d}_t = \dot{\ } \equiv \partial_t + \dot{\mathbf{x}}\cdot\nabla_{\mathbf{x}}$. In addition, the Euler equation can be recast in the form

$$\partial_t\,\dot{\mathbf{x}} + (\dot{\mathbf{x}}\cdot\nabla_{\mathbf{x}})\,\dot{\mathbf{x}} + 2H\,\dot{\mathbf{x}} = -\frac{1}{a^2}\,\Phi\,, \tag{A.3}$$

where $\Phi \equiv \phi + a\,\ddot{a}\,\mathbf{x}^2/2$ is the peculiar gravitational potential. Finally, the Poisson equation turns into

$$\frac{1}{a^2}\,\nabla_{\mathbf{x}}^2\Phi = \left(4\pi G\,\rho + 3\,\frac{\ddot{a}}{a}\right)\,, \tag{A.4}$$

where on the r.h.s. one can recognize terms that appear in the standard cosmological acceleration equation. It is convenient to take the divergence of the Euler equation, insert in it the Poisson one, and use the vector decomposition $\nabla_{\mathbf{x}}\cdot[(\dot{\mathbf{x}}\cdot\nabla_{\mathbf{x}})\,\dot{\mathbf{x}}] = (\dot{\mathbf{x}}\cdot\nabla_{\mathbf{x}})\,\theta + \frac{1}{3}\,\theta^2 + 2\,(\sigma^2 - \omega^2)$, where $\sigma \equiv \sqrt{\sigma_{ij}\sigma^{ij}/2}$ and $\omega \equiv \sqrt{\omega_{ij}\omega^{ij}/2}$ are the magnitudes of the shear σ_{ij} and rotation ω_{ij} tensors, respectively. Putting all together, one gets

$$\dot{\theta} + 2H\,\theta + \frac{\theta^2}{3} + 2\,(\sigma^2 - \omega^2) = -\left(3\frac{\ddot{a}}{a} + 4\pi G\rho\right)\,. \tag{A.5}$$

The above field equations (A.2) and (A.5) are supposed to hold at any given spatial locations, but we now proceed to take spatial averages over a comoving volume $V(t) \equiv \int \mathrm{d}^3\mathbf{x}$. First of all, one can notice that

$$
\begin{aligned}
\frac{\dot{V}}{V} &= \frac{1}{V}\,\mathrm{d}_t\int_{V(t)}\mathrm{d}^3\mathbf{x} = \frac{1}{V}\,\mathrm{d}_t\int_{V(t_0)}\mathrm{d}^3\mathbf{x_0}\,|J| = \frac{1}{V}\int_{V(t_0)}\mathrm{d}^3\mathbf{x_0}\,|\dot{J}| = \\
&= \frac{1}{V}\int_{V(t_0)}\mathrm{d}^3\mathbf{x_0}\,|J|\,\theta = \frac{1}{V}\int_{V(t)}\mathrm{d}^3\mathbf{x}\,\theta = \langle\theta\rangle\,,
\end{aligned}
\tag{A.6}
$$

where we have defined the Jacobian $J \equiv \nabla_{\mathbf{x_0}}\mathbf{x}$ and used the fact that $\dot{J} = \nabla_{\mathbf{x_0}}\dot{\mathbf{x}} = (\nabla_{\mathbf{x_0}}\dot{\mathbf{x}}/\nabla_{\mathbf{x_0}}\mathbf{x})\,\nabla_{\mathbf{x_0}}\mathbf{x} = \nabla_{\mathbf{x}}\dot{\mathbf{x}}\,\nabla_{\mathbf{x_0}}\mathbf{x} = \theta\,J$ holds (symbolic calculus employed here). Then the spatial-average and time-derivative operations of a generic field $\mathcal{F}$ are seen not to commute since

$$\langle\dot{\mathcal{F}}\rangle = \mathrm{d}_t\left(\frac{1}{V}\int_{V(t)}\mathrm{d}^3\mathbf{x}\,\mathcal{F}\right) = -\frac{\dot{V}}{V}\,\langle\mathcal{F}\rangle + \frac{1}{V}\int_{V(t_0)}\mathrm{d}^3\mathbf{x_0}\,\mathrm{d}_t(\mathcal{F}\,J) = -\langle\theta\rangle\,\langle\mathcal{F}\rangle + \langle\dot{\mathcal{F}}\rangle + \langle\mathcal{F}\theta\rangle\,. \tag{A.7}$$

Applying the averaging procedure to equations (A.2) and (A.5) we obtain

$$
\begin{cases}
\langle\dot{\theta}\rangle + 2H\,\langle\theta\rangle + \dfrac{\langle\theta\rangle^2}{3} = \dfrac{2}{3}\,\sigma_\theta^2 + 2\,(\langle\omega^2\rangle - \langle\sigma^2\rangle) - \left(3\dfrac{\ddot{a}}{a} + 4\pi G\,\langle\rho\rangle\right)\,, \\[2ex]
\langle\dot{\rho}\rangle + 3H\,\langle\rho\rangle = -\langle\rho\rangle\langle\theta\rangle\,,
\end{cases}
\tag{A.8}
$$

where $\sigma_\theta^2 \equiv \langle \theta^2 \rangle - \langle \theta \rangle^2$ is the variance of the θ field. Up to now, the background H and a have not been specified: the natural choice is to require that they represent the average scale factor and expansion rate of the spatial region; this automatically will imply that the peculiar velocity divergence $\langle \theta \rangle = 0$ is null since the average expansion of the volume will be fully described by a and H. This is also confirmed by observations of local cosmic flows, when averaging over sufficiently large scales $\gtrsim 10\, h^{-1}$ Mpc (see [49]). Putting $\langle \theta \rangle = 0$ in equation (A.8) we thus obtain

$$\begin{cases} \dfrac{\ddot{a}}{a} = -\dfrac{4\pi G}{3}\, \langle \rho \rangle + \dfrac{\mathcal{Q}}{3}\,, \\[2mm] \overset{\bullet}{\langle \rho \rangle} + 3H \,\langle \rho \rangle = 0\,, \end{cases} \tag{A.9}$$

in terms of the 'backreaction' variable $\mathcal{Q} \equiv \frac{2}{3}\, \langle \theta^2 \rangle + 2\,(\langle \omega^2 \rangle - \langle \sigma^2 \rangle)$. Integrating in time the first equation and using the second, we arrive at the spatially-averaged Friedmann equation

$$\frac{\dot{a}^2 + k}{a^2} = \frac{8\pi G}{3}\, \langle \rho \rangle + \frac{2}{3\, a^2} \int \mathrm{d}a\, a\, \mathcal{Q}\,. \tag{A.10}$$

Finally, it is convenient to redefine the density in terms of an effective matter source $\langle \rho_{\mathrm{eff}} \rangle \equiv \langle \rho \rangle + \frac{1}{4\pi G a^2} \int \mathrm{d}a\, a\, \mathcal{Q}$, that leads to the system

$$\begin{cases} \left(\dfrac{\dot{a}}{a}\right)^2 = \dfrac{8\pi G}{3}\, \langle \rho_{\mathrm{eff}} \rangle - \dfrac{k}{a^2}\,, \\[2mm] \overset{\bullet}{\langle \rho_{\mathrm{eff}} \rangle} + 3H\, \langle \rho_{\mathrm{eff}} \rangle = \dfrac{H\mathcal{Q}}{4\pi G}\, \left(1 + \dfrac{1}{a^2\, \mathcal{Q}}\, \int \mathrm{d}a\, a\, \mathcal{Q}\right)\,. \end{cases} \tag{A.11}$$

One may wonder if the constant k is somehow related to the spatially-averaged scalar curvature of the region. A general relativistic treatment of the spatial averaging procedure carried out by [67, 69–71] shows that

$$\frac{k}{a^2} = \frac{\langle \mathcal{R} \rangle + \mathcal{Q}}{6} + \frac{2}{3\, a^2} \int \mathrm{d}a\, a\, \mathcal{Q}\,, \tag{A.12}$$

holds in terms of the spatially-averaged three-dimensional Ricci scalar $\langle \mathcal{R} \rangle$. This is because inhomogeneities in the matter distribution may trigger the developments of spatially-averaged curvature also in regions that were originally close to flatness with small k (see also [76, 126]). All in all, the constant k must be thought as an initial condition related to the spatial curvature pertaining to the patch under consideration at early times (when $\mathcal{Q} \approx 0$), but this direct link with the scalar curvature is lost as inhomogeneities/anisotropies develop at late times.

Note that the backreaction term $\mathcal{Q}$ in equations (A.11) and (A.12) has been subject to a longstanding debate in the community since the early conjecture that under certain conditions it could possibly affect the expansion rate of (a region in) the Universe and led to an overall acceleration [70, 126]. On the one hand, it has been pointed out that the impact of (deterministic) backreaction depends on the size of the region, which rapidly decreases for scales larger than the largest inhomogeneity [66, 127, 128], as also indicated by numerical simulations in a general relativistic setting [129, 130]. However, these conclusions strongly rely on the assumption that it is possible to define a global background metric (or a global
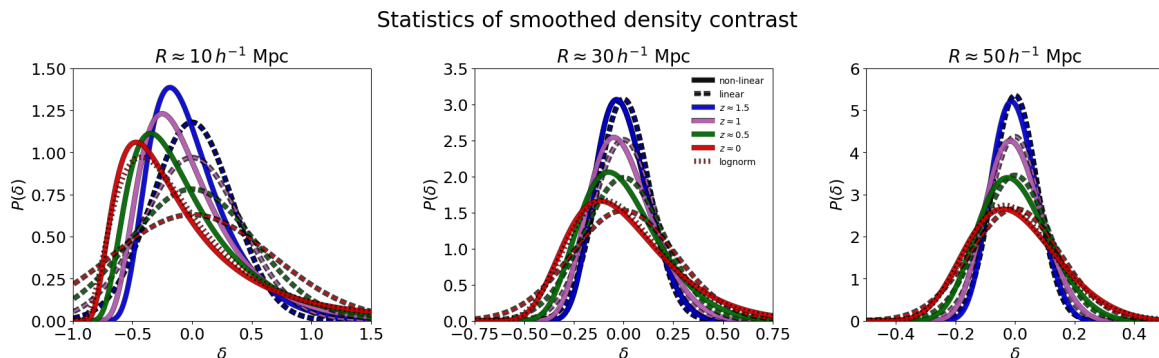
Statistics of smoothed density contrast

Figure 8. Statistics of the overdensity field smoothed on different comoving spatial scales $R \approx 10\,h^{-1}$ Mpc (left), $30\,h^{-1}$ Mpc (middle) and $50\,h^{-1}$ Mpc (right) at various redshifts $z \approx 1.5$ (blue), 1 (magenta), 0.5 (green) and 0 (red). Dashed line illustrate the outcomes from linear evolution (Gaussian shapes) and solid lines the true, non-linear distributions (approximately lognormal shapes). The red dotted line is an exactly lognormal distribution with the same mean and variance of the true one at $z \approx 0$, to highlight the slight deviation of the true distribution from the lognormal behavior. The non-linear statistics is computed via the fitting formula to numerical simulations by [47].

rescaling of it to different scales) and a deterministic backreaction term. This is not at all guaranteed at late times on scales $\lesssim 50\,h^{-1}$ Mpc pertaining to the cosmic web and relevant for several cosmological observables. There the different evolutions of the various patches due to local inhomogeneities/anisotropies, cosmic flows, tidal forces, sample variance, and many complex gravitational processes cannot be neglected and call for a statistical approach to cosmology as pursued in the main text.

To make contact between equations (A.11) and the ηCDM framework, we can (naively) proceed as follows. First of all, since the constant curvature parameter k is typically small on the large scales considered here, we can use the Friedmann equation to approximately write $H^2 \propto \langle \rho_{\rm eff} \rangle$ in the mass-energy evolution equation, to obtain

$$\langle \overset{\bullet}{\rho}_{\rm eff} \rangle + 3H \langle \rho_{\rm eff} \rangle = \frac{2}{3} \langle \rho_{\rm eff} \rangle H^{-1} \mathcal{Q} \left(1 + \frac{1}{a^2 \mathcal{Q}} \int \mathrm{d}a\, a\, \mathcal{Q} \right) . \tag{A.13}$$

Then we can have an hint on the stochastic nature of the variable $\mathcal{Q} \sim \langle \theta^2 \rangle$ from the following argument. It is well known from theoretical considerations and numerical simulations that the density contrast field $1 + \langle \delta \rangle \propto \langle \rho \rangle$ smoothed on a given large spatial scale (e.g., tens of Mpc) follows a Gaussian distribution at early times: this reflects the initial conditions that are almost preserved during linear evolution. However, at late times its distribution shifts toward an approximately lognormal shape (see [45–47]); this is because complex gravitational processes associated to nonlinear structure formation tend to aggregate matter in the filaments/nodes of the cosmic web, while subtracting it from other regions that will turn out to be the voids. In figure 8 one can visualize the late-time evolution for the statistics of the density contrast smoothed on different comoving scales $R \approx 10 - 30 - 50\,h^{-1}$ Mpc; this has been computed via the precise fitting formula to numerical simulations by [47]. It is evident, especially for scales $\lesssim 30\,h^{-1}$ Mpc that the non-linear evolution associated to structure formation kicks in at $z \lesssim 1$ to change appreciably the initial overdensity distribution, converting it from a Gaussian to a closely lognormal shape.

All the above means that sampling different large-scale patches in the late-time Universe would yield a closely lognormal distribution for the related values of $\langle\rho\rangle \propto 1 + \langle\delta\rangle$ or, equivalently, a normal distribution for $\log\langle\rho\rangle$. In terms of basic stochastic processes, such a distribution would be naturally created by an ensemble of regions whose spatially-averaged density evolves stochastically in time under a Gaussian white noise $\eta(t)$ or, in other words, for which $d_t \log\langle\rho\rangle \propto \dot{\langle\rho\rangle}/\langle\rho\rangle \propto \eta(t)$ applies (see [81, 82]; also appendix A in [1]). To realize this in equation (A.13), it is natural to assume the scaling

$$\mathcal{Q}(t) \approx \langle\theta^2\rangle \propto \langle\theta^2\rangle_\star \, H^{\alpha+1} \, \eta(t) \,, \tag{A.14}$$

where $\langle\theta^2\rangle_\star$ is the value of the peculiar divergence velocity field at a reference time, and α is a parameter (expected to be close to -1), which describes possible deviations from a pure additive noise behavior. Since in our framework the noise term associated to $\mathcal{Q} \approx \langle\theta^2\rangle \propto \eta(t)$ is meant to describe small deviations from homogeneity/isotropy, the quantity $\frac{1}{a^2}\int da\, a\, \mathcal{Q}$ entering equation (A.13) and the definition of $\langle\rho_{\text{eff}}\rangle$, where the fluctuating variable $\mathcal{Q}$ is averaged over cosmic time, could be considered of sub-leading order. This approximately implies $\langle\rho_{\text{eff}}\rangle \simeq \langle\rho\rangle$ and yields the mass-energy evolution equation

$$\dot{\langle\rho\rangle} + 3H\langle\rho\rangle = \zeta\langle\rho\rangle \left(\frac{H}{H_\star}\right)^\alpha H_\star^{1/2}\eta(t)\,, \tag{A.15}$$

where the adimensional parameter $\zeta \propto \langle\theta^2\rangle_\star$ encases all the proportionality constants, and $H_\star$ is an arbitrary reference value of the Hubble parameter which ensures dimensional consistency since the noise η has dimension of $1/\sqrt{\text{time}}$. In fact, a stochastic equation of such form is adopted in the ηCDM model.

Plainly, the strength parameter $\zeta \propto \langle\theta^2\rangle_\star$ is related to the spatially-averaged variance of the divergence of the peculiar velocity field, and will depend on the smoothing scale. Over the size of the whole Universe, one should expect $\zeta \propto \langle\theta^2\rangle \approx 0$, and so there will be no impact of the stochasticity. However, on scales $R \lesssim 50\,h^{-1}$ Mpc associated to the emergence of the cosmic web, that are crucial to many cosmological data, the value of $\zeta \propto \langle\theta^2\rangle$ can be non-negligible. This occurrence will bring about a relevant impact of the stochasticity in the overall late-time cosmological evolution.

To summarize, although in the original ηCDM model by [1] the stochasticity in the mass-energy evolution equation was somewhat postulated or at most justified only qualitatively, the above lines of reasoning show that it can be actually understood in the context of spatial averaging in Newtonian cosmology, and its scale-dependent strength $\zeta \propto \langle\theta^2\rangle_\star$ can be quantitatively related to the value of the spatially-averaged variance of the divergence of the peculiar velocity field. It will be extremely interesting to precisely measure the latter from reconstruction of the cosmic velocity pattern.

B Growth of linear perturbations in ηCDM

In this appendix we derive the equation for the evolution of linear perturbations in the ηCDM model. One can start by writing $\langle\rho\rangle \simeq \rho_0\,(1 + \delta)$ in equation (A.8) where δ is a small perturbation in any given patch of background density ρ_0. An important point to recall is that

$\theta \equiv \nabla_{\mathbf{x}} \cdot \dot{\mathbf{x}}$ is the divergence of the peculiar velocity field and hence is also small (same order of δ, see below). This implies that the backreaction variable $\mathcal{Q} \sim \langle \theta^2 \rangle$ can be neglected at linear order, hence no stochasticity enters into the game and all the patches (and plainly also the ensemble average) would evolve in the same way; up to the linear regime there is no difference with respect to the standard cosmological evolution. In fact, at zeroth order one gets the standard Friedmann equations for an Einstein de Sitter Universe, while at first order one has

$$\begin{cases} \dot{\theta} + 2H\,\theta = -4\pi\,G\,\rho_0\,\delta\,, \\ \dot{\delta} \simeq -\theta\,, \end{cases} \tag{B.1}$$

or equivalently

$$\ddot{\delta} + 2H\,\dot{\delta} = 4\pi G\,\rho_0\,\delta\,. \tag{B.2}$$

Passing to log-conformal time $\mathrm{d}\ln a = H\,\mathrm{d}t$ and indicating with a prime the derivatives with respect to $\ln a$, one obtains

$$\delta'' + \left(2 + \frac{H'}{H}\right)\delta' = \frac{3}{2}\,\Omega_m\,\delta\,, \tag{B.3}$$

which is equation (3.2) of the main text. As for the smoothed velocity field divergence, from the second of equations (B.1) one finds that

$$\theta = -\delta\,H\,f\,, \tag{B.4}$$

where $f(a) \equiv \delta'/\delta$ is the growth rate of perturbations in linear theory.

A subtle point in ηCDM (but also occurring in other scenarios of modified gravity) is that the zeroth order solution in perturbation theory is substantially different from the non-perturbative ensemble-averaged evolution of the Universe analyzed in the main text. This is because, as noted above, up to linear order stochasticity is negligible, so all patches of the Universe (and their ensemble average) would evolve similarly and no relevant effects, including the emergence of dark energy, would occur. However, it is more reasonable to compute the evolution of perturbations over the true non-perturbative ensemble-averaged background of the ηCDM model, which is induced by nonlinear structure formation. Thus when exploiting the equation of linear perturbations derived above, we use as background the ensemble-averaged evolution of the Hubble parameter $\bar{H}$ and of the matter density parameter $\bar{\Omega}_m$ found by solving in full equations (2.3).

The growing mode solution $\delta_+(z)$ of equation (B.1) normalized to the present time is illustrated in figure 9, while the inset shows the corresponding growth rate $f(a) = \mathrm{d}\ln\delta_+/\mathrm{d}\ln a$. Cyan solid lines refer to ΛCDM and orange solid lines to ηCDM. For reference we have assumed the same sets of cosmological parameters of figure 1 in the main text. It is seen that the growth of perturbation in ηCDM is slower than in ΛCDM; this would yield less abundant, but more massive structures at high redshift in the former with respect to the latter. It would be interesting to investigate the consequence of such a slower growth rate in ηCDM on the halo mass function, and check whether it could help explaining the overabundance of massive galaxies at high z as found by JWST surveys (e.g., [131, 132]); we plan to investigate the issue in the near future.
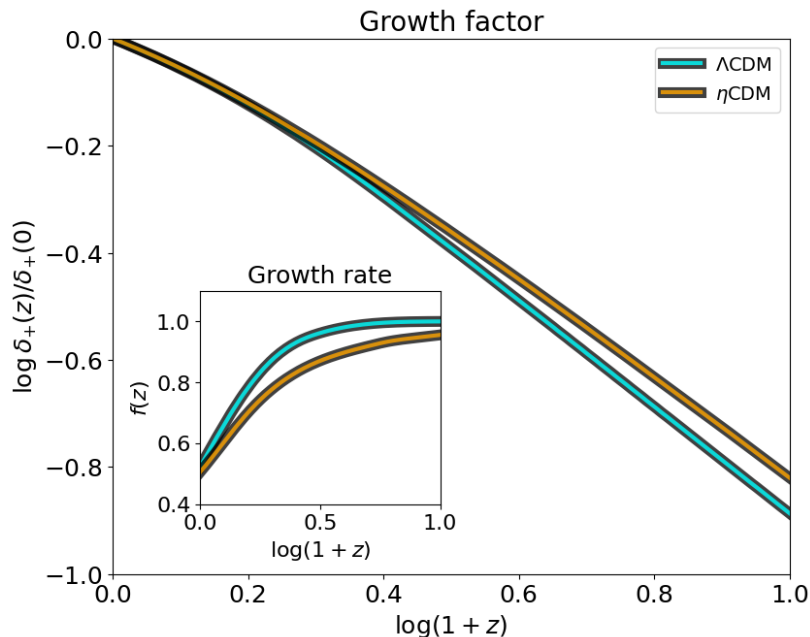
Figure 9. The growing mode solution $\delta_+(z)$ of equation (B.1) normalized to the present time as a function of redshift; the inset reports the redshift evolution of the corresponding growth rate $f(a) = \mathrm{d} \ln \delta_+ / \mathrm{d} \ln a$. Cyan solid lines refer to ΛCDM and orange solid lines to ηCDM. For reference the same sets of cosmological parameters of figure 1 have been adopted.

In ΛCDM it is well known (e.g., [115]) that a good approximation to the growth rate is given by $f(a) \simeq \Omega_m^\gamma(a)$, where the value $\gamma \approx 0.55$ of the 'growth index' is obtained when assuming standard general relativity [133–136]. In the ηCDM model we have found that the growth rate can be very well approximated as

$$f(a) \simeq \Omega_m^{\gamma(a)}(a), \tag{B.5}$$

in terms of a slowly evolving growth index $\gamma(a) \approx 0.55 + 0.15\,a$; this could be thought as a late-time deviation from the ΛCDM value $\gamma \approx 0.55$ applying at high redshift, where the initial conditions to solve equation (B.1) have been set. Remarkably, the outcome is in extremely good agreement with the recent claims for a larger value of $\gamma \gtrsim 0.64$ presented in [137], who quote a highly significant tension with the concordance cosmology. In fact, the deviation of the growth index from the standard value $\gamma \approx 0.55$ is usually interpreted as an evidence in favour of modified gravity scenarios [136, 138]. However, in the ηCDM models such steepening of the growth index toward low z can be easily explained without invoking any modifications to the fundamental nature of gravity.

Finally, the redsfhit dependence of the growth index is such that it starts to deviate from the standard value $\gamma \approx 0.55$ well within the matter-dominated regime, at around $z \lesssim 1$. Incidentally, this is around the cosmic epoch where the CMB lensing kernel peaks; in fact, a higher γ as found in ηCDM immediately implies a higher CMB lensing amplitude [137]. This is in fact consistent with observations and constitutes the well established, albeit mild, A_{lens}-or lensing-anomaly of the ΛCDM scenario [5, 139]. All in all, this could provide a hint that the

ηCDM is able to solve yet another cosmic tension. Although a clear-cut demonstration for the superior performances of the ηCDM model over the standard scenario is still far away, the above clue adds to the many assessments presented so far in this work to provide a positive outlook for future investigations of our stochastic approach to cosmology.

References

[1] A. Lapi et al., *Little Ado about Everything: ηCDM, a Cosmological Model with Fluctuation-driven Acceleration at Late Times*, *Astrophys. J.* **959** (2023) 83 [arXiv:2310.06028] [INSPIRE].

[2] WMAP collaboration, *Nine-Year Wilkinson Microwave Anisotropy Probe (WMAP) Observations: Final Maps and Results*, *Astrophys. J. Suppl.* **208** (2013) 20 [arXiv:1212.5225] [INSPIRE].

[3] ACT collaboration, *The Atacama Cosmology Telescope: DR4 Maps and Cosmological Parameters*, *JCAP* **12** (2020) 047 [arXiv:2007.07288] [INSPIRE].

[4] SPT-3G collaboration, *Measurements of the E-mode polarization and temperature-E-mode correlation of the CMB from SPT-3G 2018 data*, *Phys. Rev. D* **104** (2021) 022003 [arXiv:2101.01684] [INSPIRE].

[5] PLANCK collaboration, *Planck 2018 results. VI. Cosmological parameters*, *Astron. Astrophys.* **641** (2020) A6 [*Erratum ibid.* **652** (2021) C4] [arXiv:1807.06209] [INSPIRE].

[6] SUPERNOVA COSMOLOGY PROJECT collaboration, *Measurements of Ω and Λ from 42 High Redshift Supernovae*, *Astrophys. J.* **517** (1999) 565 [astro-ph/9812133] [INSPIRE].

[7] PAN-STARRS1 collaboration, *The Complete Light-curve Sample of Spectroscopically Confirmed SNe Ia from Pan-STARRS1 and Cosmological Constraints from the Combined Pantheon Sample*, *Astrophys. J.* **859** (2018) 101 [arXiv:1710.00845] [INSPIRE].

[8] D. Brout et al., *The Pantheon+ Analysis: Cosmological Constraints*, *Astrophys. J.* **938** (2022) 110 [arXiv:2202.04077] [INSPIRE].

[9] DES collaboration, *The Dark Energy Survey: Cosmology Results with ∼1500 New High-redshift Type Ia Supernovae Using the Full 5 yr Data Set*, *Astrophys. J. Lett.* **973** (2024) L14 [arXiv:2401.02929] [INSPIRE].

[10] BOSS collaboration, *Cosmological implications of baryon acoustic oscillation measurements*, *Phys. Rev. D* **92** (2015) 123516 [arXiv:1411.1074] [INSPIRE].

[11] BOSS collaboration, *The clustering of galaxies in the completed SDSS-III Baryon Oscillation Spectroscopic Survey: cosmological analysis of the DR12 galaxy sample*, *Mon. Not. Roy. Astron. Soc.* **470** (2017) 2617 [arXiv:1607.03155] [INSPIRE].

[12] eBOSS collaboration, *Completed SDSS-IV extended Baryon Oscillation Spectroscopic Survey: Cosmological implications from two decades of spectroscopic surveys at the Apache Point Observatory*, *Phys. Rev. D* **103** (2021) 083533 [arXiv:2007.08991] [INSPIRE].

[13] DESI collaboration, *DESI 2024 VI: cosmological constraints from the measurements of baryon acoustic oscillations*, *JCAP* **02** (2025) 021 [arXiv:2404.03002] [INSPIRE].

[14] C. Blake et al., *The WiggleZ Dark Energy Survey: Joint measurements of the expansion and growth history at z < 1*, *Mon. Not. Roy. Astron. Soc.* **425** (2012) 405 [arXiv:1204.3674] [INSPIRE].

[15] F. Beutler et al., *The 6dF Galaxy Survey: $z \approx 0$ measurement of the growth rate and σ_8*, *Mon. Not. Roy. Astron. Soc.* **423** (2012) 3430 [`arXiv:1204.4725`] [InSPIRE].

[16] T. Okumura et al., *The Subaru FMOS galaxy redshift survey (FastSound). IV. New constraint on gravity theory from redshift space distortions at $z \sim 1.4$*, *Publ. Astron. Soc. Jap.* **68** (2016) 38 [`arXiv:1511.08083`] [InSPIRE].

[17] A. Pezzotta et al., *The VIMOS Public Extragalactic Redshift Survey (VIPERS): The growth of structure at $0.5 < z < 1.2$ from redshift-space distortions in the clustering of the PDR-2 final sample*, *Astron. Astrophys.* **604** (2017) A33 [`arXiv:1612.05645`] [InSPIRE].

[18] K. Said et al., *Joint analysis of 6dFGS and SDSS peculiar velocities for the growth rate of cosmic structure and tests of gravity*, *Mon. Not. Roy. Astron. Soc.* **497** (2020) 1275 [`arXiv:2007.04993`] [InSPIRE].

[19] M.S. Turner, *The Road to Precision Cosmology*, `arXiv:2201.04741` [`DOI:10.1146/annurev-nucl-111119-041046`] [InSPIRE].

[20] S.D.M. White, J.F. Navarro, A.E. Evrard and C.S. Frenk, *The baryon content of galaxy clusters: A challenge to cosmological orthodoxy*, *Nature* **366** (1993) 429 [InSPIRE].

[21] SPT collaboration, *Cosmological constraints from gas mass fractions of massive, relaxed galaxy clusters*, *Mon. Not. Roy. Astron. Soc.* **510** (2021) 131 [`arXiv:2111.09343`] [InSPIRE].

[22] V. Ghirardini et al., *The SRG/eROSITA all-sky survey: Cosmology constraints from cluster abundances in the western Galactic hemisphere*, *Astron. Astrophys.* **689** (2024) A298 [`arXiv:2402.08458`] [InSPIRE].

[23] SUPERNOVA SEARCH TEAM collaboration, *Observational evidence from supernovae for an accelerating universe and a cosmological constant*, *Astron. J.* **116** (1998) 1009 [`astro-ph/9805201`] [InSPIRE].

[24] D. Scolnic et al., *The Pantheon+ Analysis: The Full Data Set and Light-curve Release*, *Astrophys. J.* **938** (2022) 113 [`arXiv:2112.03863`] [InSPIRE].

[25] Y.B. Zel'dovich, A. Krasinski and Y.B. Zeldovich, *The cosmological constant and the theory of elementary particles*, *Sov. Phys. Usp.* **11** (1968) 381 [InSPIRE].

[26] S. Weinberg, *The Cosmological Constant Problem*, *Rev. Mod. Phys.* **61** (1989) 1 [InSPIRE].

[27] E.Ó. Colgáin and M.M. Sheikh-Jabbari, *DESI and SNe: Dynamical Dark Energy, Ω_m Tension or Systematics?*, `arXiv:2412.12905` [InSPIRE].

[28] E.Ó. Colgáin et al., *Does DESI 2024 Confirm ΛCDM?*, `arXiv:2404.08633` [InSPIRE].

[29] A. Sousa-Neto, C. Bengaly, J.E. González and J. Alcaniz, *No evidence for dynamical dark energy from DESI and SN data: a symbolic regression analysis*, `arXiv:2502.10506` [InSPIRE].

[30] A.G. Riess et al., *A 2.4% Determination of the Local Value of the Hubble Constant*, *Astrophys. J.* **826** (2016) 56 [`arXiv:1604.01424`] [InSPIRE].

[31] A.G. Riess et al., *A Comprehensive Measurement of the Local Value of the Hubble Constant with 1 km s^{-1} Mpc^{-1} Uncertainty from the Hubble Space Telescope and the SH0ES Team*, *Astrophys. J. Lett.* **934** (2022) L7 [`arXiv:2112.04510`] [InSPIRE].

[32] A.G. Riess et al., *JWST Validates HST Distance Measurements: Selection of Supernova Subsample Explains Differences in JWST Estimates of Local H_0*, *Astrophys. J.* **977** (2024) 120 [`arXiv:2408.11770`] [InSPIRE].

[33] C. Heymans et al., *CFHTLenS tomographic weak lensing cosmological parameter constraints: Mitigating the impact of intrinsic galaxy alignments*, *Mon. Not. Roy. Astron. Soc.* **432** (2013) 2433 [arXiv:1303.1808] [INSPIRE].

[34] E. Di Valentino et al., *Cosmology Intertwined III: $f\sigma_8$ and S_8*, *Astropart. Phys.* **131** (2021) 102604 [arXiv:2008.11285] [INSPIRE].

[35] DES collaboration, *Dark Energy Survey Year 3 results: Cosmology from cosmic shear and robustness to modeling uncertainty*, *Phys. Rev. D* **105** (2022) 023515 [arXiv:2105.13544] [INSPIRE].

[36] A. Amon and G. Efstathiou, *A non-linear solution to the S_8 tension?*, *Mon. Not. Roy. Astron. Soc.* **516** (2022) 5355 [arXiv:2206.11794] [INSPIRE].

[37] P.K. Aluri et al., *Is the observable Universe consistent with the cosmological principle?*, *Class. Quant. Grav.* **40** (2023) 094001 [arXiv:2207.05765] [INSPIRE].

[38] H.M. Courtois et al., *In search for the Local Universe dynamical homogeneity scale with CF4++ peculiar velocities*, arXiv:2502.01308 [INSPIRE].

[39] D.W. Pesce et al., *The Megamaser Cosmology Project. XIII. Combined Hubble constant constraints*, *Astrophys. J. Lett.* **891** (2020) L1 [arXiv:2001.09213] [INSPIRE].

[40] S.S. Boruah, M.J. Hudson and G. Lavaux, *Cosmic flows in the nearby Universe: new peculiar velocities from SNe and cosmological constraints*, *Mon. Not. Roy. Astron. Soc.* **498** (2020) 2703 [arXiv:1912.09383] [INSPIRE].

[41] R.B. Tully et al., *Cosmicflows-4*, *Astrophys. J.* **944** (2023) 94 [arXiv:2209.11238] [INSPIRE].

[42] N.I. Libeskind et al., *Tracing the cosmic web*, *Mon. Not. Roy. Astron. Soc.* **473** (2018) 1195 [arXiv:1705.03021] [INSPIRE].

[43] G. Wilding et al., *Persistent homology of the cosmic web — I. Hierarchical topology in ΛCDM cosmologies*, *Mon. Not. Roy. Astron. Soc.* **507** (2021) 2968 [arXiv:2011.12851] [INSPIRE].

[44] K.A. Douglass, D. Veyrat and S. BenZvi, *Updated Void Catalogs of the SDSS DR7 Main Sample*, *Astrophys. J. Suppl.* **265** (2023) 7 [arXiv:2202.01226] [INSPIRE].

[45] P. Coles and B. Jones, *A lognormal model for the cosmological mass distribution*, Mon. Not. Roy. Astron. Soc. **248** (1991) 1 [INSPIRE].

[46] A. Repp and I. Szapudi, *Precision Prediction of the Log Power Spectrum*, *Mon. Not. Roy. Astron. Soc.* **464** (2017) L21 [arXiv:1607.01386] [INSPIRE].

[47] A. Repp and I. Szapudi, *The Bias of the Log Power Spectrum for Discrete Surveys*, *Mon. Not. Roy. Astron. Soc.* **475** (2018) L6 [arXiv:1708.00954] [INSPIRE].

[48] R.B. Tully et al., *Our Peculiar Motion Away from the Local Void*, *Astrophys. J.* **676** (2008) 184 [arXiv:0705.4139] [INSPIRE].

[49] Y. Hoffman et al., *The large scale velocity field from the Cosmicflows-4 data*, arXiv:2311.01340 [INSPIRE].

[50] G. Bertone and M.P.T. Tait, *A new era in the search for dark matter*, *Nature* **562** (2018) 51 [arXiv:1810.01668] [INSPIRE].

[51] J. Ellis and D. Wands, *Inflation (2023)*, arXiv:2312.13238 [INSPIRE].

[52] P.J.E. Peebles, *Nobel Lecture: How physical cosmology grew*, *Rev. Mod. Phys.* **92** (2020) 030501 [INSPIRE].

[53] G. Efstathiou, *Do we have a standard model of cosmology?*, *Astron. Geophys.* **64** (2023) 1.21.

[54] T. Clifton, P.G. Ferreira, A. Padilla and C. Skordis, *Modified Gravity and Cosmology*, *Phys. Rept.* **513** (2012) 1 [arXiv:1106.2476] [INSPIRE].

[55] S. Nojiri, S.D. Odintsov and V.K. Oikonomou, *Modified Gravity Theories on a Nutshell: Inflation, Bounce and Late-time Evolution*, *Phys. Rept.* **692** (2017) 1 [arXiv:1705.11098] [INSPIRE].

[56] CANTATA collaboration, *Modified Gravity and Cosmology. An Update by the CANTATA Network*, Springer (2021) [DOI:10.1007/978-3-030-83715-0] [INSPIRE].

[57] K. Freese and M. Lewis, *Cardassian expansion: A model in which the universe is flat, matter dominated, and accelerating*, *Phys. Lett. B* **540** (2002) 1 [astro-ph/0201229] [INSPIRE].

[58] L. Xu, *Revisiting Cardassian Model and Cosmic Constraint*, *Eur. Phys. J. C* **72** (2012) 2134 [arXiv:1208.3715] [INSPIRE].

[59] J. Magaña, M.H. Amante, M.A. García-Aspeitia and V. Motta, *The Cardassian expansion revisited: constraints from updated Hubble parameter measurements and type Ia supernova data*, *Mon. Not. Roy. Astron. Soc.* **476** (2018) 1036 [arXiv:1706.09848] [INSPIRE].

[60] J.A.S. Lima, R. Portugal and I. Waga, *Bulk-viscosity-driven asymmetric inflationary universe*, *Phys. Rev. D* **37** (1988) 2755 [INSPIRE].

[61] I. Brevik, E. Elizalde, S. Nojiri and S.D. Odintsov, *Viscous Little Rip Cosmology*, *Phys. Rev. D* **84** (2011) 103508 [arXiv:1107.4642] [INSPIRE].

[62] L. Herrera-Zamorano, M.A. García-Aspeitia and A. Hernández-Almada, *Constraints and cosmography of ΛCDM in presence of viscosity*, *Eur. Phys. J. C* **80** (2020) 637 [arXiv:2007.04507] [INSPIRE].

[63] M.-N. Célérier, *Do we really see a cosmological constant in the supernovae data?*, *Astron. Astrophys.* **353** (2000) 63 [astro-ph/9907206] [INSPIRE].

[64] H. Alnes, M. Amarzguioui and Ø. Grøn, *An inhomogeneous alternative to dark energy?*, *Phys. Rev. D* **73** (2006) 083519 [astro-ph/0512006] [INSPIRE].

[65] V. Deledicque, *Development of a model to investigate the effect of the bias in SNIa measurements related to the inhomogeneity of space*, *Eur. Phys. J. C* **83** (2023) 566 [arXiv:2302.11938] [INSPIRE].

[66] T. Buchert and J. Ehlers, *Averaging inhomogeneous Newtonian cosmologies*, *Astron. Astrophys.* **320** (1997) 1 [astro-ph/9510056] [INSPIRE].

[67] T. Buchert, M. Kerscher and C. Sicka, *Back reaction of inhomogeneities on the expansion: The evolution of cosmological parameters*, *Phys. Rev. D* **62** (2000) 043525 [astro-ph/9912347] [INSPIRE].

[68] T. Buchert, *On average properties of inhomogeneous fluids in general relativity. 1. Dust cosmologies*, *Gen. Rel. Grav.* **32** (2000) 105 [gr-qc/9906015] [INSPIRE].

[69] T. Buchert, *Dark Energy from Structure: A Status Report*, *Gen. Rel. Grav.* **40** (2008) 467 [arXiv:0707.2153] [INSPIRE].

[70] T. Buchert and S. Räsänen, *Backreaction in late-time cosmology*, *Ann. Rev. Nucl. Part. Sci.* **62** (2012) 57 [arXiv:1112.5335] [INSPIRE].

[71] T. Buchert, C. Nayet and A. Wiegand, *Lagrangian theory of structure formation in relativistic cosmology II: average properties of a generic evolution model*, *Phys. Rev. D* **87** (2013) 123503 [arXiv:1303.6193] [INSPIRE].

[72] S. Räsänen, *Light propagation in statistically homogeneous and isotropic universes with general matter content*, *JCAP* **03** (2010) 018 [`arXiv:0912.3370`] [InSPIRE].

[73] G. Rácz et al., *Concordance cosmology without dark energy*, *Mon. Not. Roy. Astron. Soc.* **469** (2017) L1 [`arXiv:1607.08797`] [InSPIRE].

[74] S.M. Koksbang, *Observations in statistically homogeneous, locally inhomogeneous cosmological toy-models without FLRW backgrounds*, *Mon. Not. Roy. Astron. Soc.* **498** (2020) L135 [`arXiv:2008.07108`] [InSPIRE].

[75] S. Schander and T. Thiemann, *Backreaction in Cosmology*, *Front. Astron. Space Sci.* **0** (2021) 113 [`arXiv:2106.06043`] [InSPIRE].

[76] D.L. Wiltshire, *Exact solution to the averaging problem in cosmology*, *Phys. Rev. Lett.* **99** (2007) 251101 [`arXiv:0709.0732`] [InSPIRE].

[77] D.L. Wiltshire, *Average observational quantities in the timescape cosmology*, *Phys. Rev. D* **80** (2009) 123512 [`arXiv:0909.0749`] [InSPIRE].

[78] A. Seifert et al., *Supernovae evidence for foundational change to cosmological models*, *Mon. Not. Roy. Astron. Soc.* **537** (2025) L55 [`arXiv:2412.15143`] [InSPIRE].

[79] S.M. Koksbang, *Testing inhomogeneous cosmography in our cosmic neighborhood using CosmicFlows-4*, `arXiv:2412.12637` [InSPIRE].

[80] H.J. Macpherson, *The Impact of Anisotropic Sky Sampling on the Hubble Constant in Numerical Relativity*, *Astrophys. J.* **970** (2024) 111 [`arXiv:2402.09659`] [InSPIRE].

[81] H. Risken, *The Fokker-Planck Equation: Methods of Solution and Applications*, Springer Berlin Heidelberg (1996) [`DOI:10.1007/978-3-642-61544-3`].

[82] W. Paul and J. Baschnagel, *Stochastic Processes: From Physics to Finance*, Springer International Publishing (2013) [`DOI:10.1007/978-3-319-00327-6`].

[83] A. Vilenkin, *The Birth of Inflationary Universes*, *Phys. Rev. D* **27** (1983) 2848 [InSPIRE].

[84] D.S. Salopek and J.R. Bond, *Stochastic inflation and nonlinear gravity*, *Phys. Rev. D* **43** (1991) 1005 [InSPIRE].

[85] D. Cruces, *Review on Stochastic Approach to Inflation*, *Universe* **8** (2022) 334 [`arXiv:2203.13852`] [InSPIRE].

[86] J.R. Bond, S. Cole, G. Efstathiou and N. Kaiser, *Excursion set mass functions for hierarchical Gaussian fluctuations*, *Astrophys. J.* **379** (1991) 440 [InSPIRE].

[87] H.J. Mo and S.D.M. White, *An analytic model for the spatial clustering of dark matter halos*, *Mon. Not. Roy. Astron. Soc.* **282** (1996) 347 [`astro-ph/9512127`] [InSPIRE].

[88] A. Lapi and L. Danese, *A Stochastic Theory of the Hierarchical Clustering I. Halo Mass Function*, *Astrophys. J.* **903** (2020) 117 [`arXiv:2009.07023`] [InSPIRE].

[89] A. Lapi, T. Ronconi and L. Danese, *A Stochastic Theory of the Hierarchical Clustering. III. The Nonuniversality and Nonstationarity of the Halo Mass Function*, *Astrophys. J.* **941** (2022) 14 [`arXiv:2211.00399`] [InSPIRE].

[90] J. Neyman, *Alternative Stochastic Models of the Spatial Distribution of Galaxies*, *Problems of Extra-Galactic Research* **15** (1962) 294.

[91] P.J.E. Peebles, *Anomalies in physical cosmology*, *Annals Phys.* **447** (2022) 169159 [`arXiv:2208.05018`] [InSPIRE].

[92] M.J. Williams, H.J. Macpherson, D.L. Wiltshire and C. Stevens, *First investigation of void statistics in numerical relativity simulations*, *Mon. Not. Roy. Astron. Soc.* **536** (2024) 2645 [arXiv:2403.15134] [INSPIRE].

[93] T. Buchert, A. Domínguez and J. Pérez-Mercader, *Extending the scope of models for large scale structure formation in the universe*, *Astron. Astrophys.* **349** (1999) 343 [astro-ph/9709218] [INSPIRE].

[94] K. Bolejko, *Emerging spatial curvature can resolve the tension between high-redshift CMB and low-redshift distance ladder measurements of the Hubble constant*, *Phys. Rev. D* **97** (2018) 103529 [arXiv:1712.02967] [INSPIRE].

[95] R. Mainini and S. Bonometto, *Dark Matter and Dark Energy from a single scalar field: CMB spectrum and matter transfer function*, *JCAP* **09** (2007) 017 [arXiv:0709.0174] [INSPIRE].

[96] E. Di Valentino, A. Melchiorri, O. Mena and S. Vagnozzi, *Interacting dark energy in the early 2020s: A promising solution to the H_0 and cosmic shear tensions*, *Phys. Dark Univ.* **30** (2020) 100666 [arXiv:1908.04281] [INSPIRE].

[97] A. Aich, *Interacting Dark Energy: New Parametrization and Observational Constraints*, *Astron. Rep.* **67** (2023) 537 [arXiv:2207.09079] [INSPIRE].

[98] M.A. van der Westhuizen and A. Abebe, *Interacting dark energy: clarifying the cosmological implications and viability conditions*, *JCAP* **01** (2024) 048 [arXiv:2302.11949] [INSPIRE].

[99] J. Gleyzes, D. Langlois, M. Mancarella and F. Vernizzi, *Effective Theory of Interacting Dark Energy*, *JCAP* **08** (2015) 054 [arXiv:1504.05481] [INSPIRE].

[100] D. Benisty and E.I. Guendelman, *Unified dark energy and dark matter from dynamical spacetime*, *Phys. Rev. D* **98** (2018) 023506 [arXiv:1802.07981] [INSPIRE].

[101] F.K. Anagnostopoulos, D. Benisty, S. Basilakos and E.I. Guendelman, *Dark energy and dark matter unification from dynamical space time: observational constraints and cosmological implications*, *JCAP* **06** (2019) 003 [arXiv:1904.05762] [INSPIRE].

[102] W. Giarè et al., *Tightening the reins on nonminimal dark sector physics: Interacting dark energy with dynamical and nondynamical equation of state*, *Phys. Rev. D* **110** (2024) 063527 [arXiv:2404.02110] [INSPIRE].

[103] S.M. Koksbang, *Another look at redshift drift and the backreaction conjecture*, *JCAP* **10** (2019) 036 [arXiv:1909.13489] [INSPIRE].

[104] S.M. Koksbang, *Towards statistically homogeneous and isotropic perfect fluid universes with cosmic backreaction*, *Class. Quant. Grav.* **36** (2019) 185004 [arXiv:1907.08681] [INSPIRE].

[105] M. Visser, *Cosmography: Cosmology without the Einstein equations*, *Gen. Rel. Grav.* **37** (2005) 1541 [gr-qc/0411131] [INSPIRE].

[106] S. Capozziello, R. Lazkoz and V. Salzano, *Comprehensive cosmographic analysis by Markov Chain Method*, *Phys. Rev. D* **84** (2011) 124061 [arXiv:1104.3096] [INSPIRE].

[107] S. Nesseris, G. Pantazis and L. Perivolaropoulos, *Tension and constraints on modified gravity parametrizations of $G_{eff}(z)$ from growth rate and Planck data*, *Phys. Rev. D* **96** (2017) 023542 [arXiv:1703.10538] [INSPIRE].

[108] M. Moresco, *Measuring the expansion history of the Universe with cosmic chronometers*, arXiv:2412.01994 [INSPIRE].

[109] M. Moresco et al., *Unveiling the Universe with emerging cosmological probes*, *Living Rev. Rel.* **25** (2022) 6 [arXiv:2201.07241] [INSPIRE].

[110] D. Valcin et al., *The age of the Universe with globular clusters: reducing systematic uncertainties*, *JCAP* **08** (2021) 017 [arXiv:2102.04486] [INSPIRE].

[111] D. Foreman-Mackey, D.W. Hogg, D. Lang and J. Goodman, *emcee: The MCMC Hammer*, *Publ. Astron. Soc. Pac.* **125** (2013) 306 [arXiv:1202.3665] [INSPIRE].

[112] U. Mukhopadhyay, S. Haridasu, A.A. Sen and S. Dhawan, *Inferring dark energy properties from the scale factor parametrization*, *Phys. Rev. D* **110** (2024) 123516 [arXiv:2407.10845] [INSPIRE].

[113] V. Marra, *Coupling dark energy to dark matter inhomogeneities*, *Phys. Dark Univ.* **13** (2016) 25 [arXiv:1506.05523] [INSPIRE].

[114] M. Chevallier and D. Polarski, *Accelerating universes with scaling dark matter*, *Int. J. Mod. Phys. D* **10** (2001) 213 [gr-qc/0009008] [INSPIRE].

[115] E.V. Linder, *Exploring the expansion history of the universe*, *Phys. Rev. Lett.* **90** (2003) 091301 [astro-ph/0208512] [INSPIRE].

[116] E.V. Linder, *Cosmic Growth and Expansion Conjoined*, *Astropart. Phys.* **86** (2017) 41 [arXiv:1610.05321] [INSPIRE].

[117] S.M. Koksbang, *Searching for signals of inhomogeneity using multiple probes of the cosmic expansion rate H(z)*, *Phys. Rev. Lett.* **126** (2021) 231101 [arXiv:2105.11880] [INSPIRE].

[118] KiDS collaboration, *KiDS-1000 Cosmology: Cosmic shear constraints and comparison between two point statistics*, *Astron. Astrophys.* **645** (2021) A104 [arXiv:2007.15633] [INSPIRE].

[119] DES collaboration, *Dark Energy Survey Year 3 results: Cosmology from cosmic shear and robustness to data calibration*, *Phys. Rev. D* **105** (2022) 023514 [arXiv:2105.13543] [INSPIRE].

[120] A.M. Lopez, R.G. Clowes and G.M. Williger, *A Giant Arc on the Sky*, *Mon. Not. Roy. Astron. Soc.* **516** (2022) 1557 [arXiv:2201.06875] [INSPIRE].

[121] A.M. Lopez, R.G. Clowes and G.M. Williger, *A Big Ring on the sky*, *JCAP* **07** (2024) 055 [arXiv:2402.07591] [INSPIRE].

[122] H. Boehringer et al., *Unveiling the largest structures in the nearby Universe: Discovery of the Quipu superstructure*, *Astron. Astrophys.* **695** (2025) A59 [arXiv:2501.19236] [INSPIRE].

[123] B.F. Roukema, *Replacing dark energy by silent virialisation*, *Astron. Astrophys.* **610** (2018) A51 [arXiv:1706.06179] [INSPIRE].

[124] S.L. Cacciatori, V. Gorini and F. Re, *Dark Energy*, arXiv:2410.10435 [DOI:10.1007/978-3-031-61187-2_13] [INSPIRE].

[125] M. Vogelsberger, F. Marinacci, P. Torrey and E. Puchwein, *Cosmological Simulations of Galaxy Formation*, *Nature Rev. Phys.* **2** (2020) 42 [arXiv:1909.07976] [INSPIRE].

[126] E.W. Kolb, *Backreaction of inhomogeneities can mimic dark energy*, *Class. Quant. Grav.* **28** (2011) 164009 [INSPIRE].

[127] N. Kaiser, *Why there is no Newtonian backreaction*, *Mon. Not. Roy. Astron. Soc.* **469** (2017) 744 [arXiv:1703.08809] [INSPIRE].

[128] T. Buchert, *On backreaction in Newtonian cosmology*, *Mon. Not. Roy. Astron. Soc.* **473** (2018) L46 [arXiv:1704.00703] [INSPIRE].

[129] J. Adamek et al., *Safely smoothing spacetime: backreaction in relativistic cosmological simulations*, *Class. Quant. Grav.* **36** (2019) 014001 [arXiv:1706.09309] [INSPIRE].

[130] H.J. Macpherson, D.J. Price and P.D. Lasky, *Einstein's Universe: Cosmological structure formation in numerical relativity*, *Phys. Rev. D* **99** (2019) 063522 [`arXiv:1807.01711`] [ɪɴSPIRE].

[131] I. Labbé et al., *A population of red candidate massive galaxies ∼600 Myr after the Big Bang*, *Nature* **616** (2023) 266 [`arXiv:2207.12446`] [ɪɴSPIRE].

[132] R. Jain and Y. Wadadekar, *A grand-design spiral galaxy 1.5 billion years after the Big Bang with JWST*, `arXiv:2412.04834`.

[133] J.N. Fry, *Dynamical Measures of Density in Exotic Cosmologies*, *Phys. Lett. B* **158** (1985) 211 [ɪɴSPIRE].

[134] E.V. Linder, *Cosmic growth history and expansion history*, *Phys. Rev. D* **72** (2005) 043529 [`astro-ph/0507263`] [ɪɴSPIRE].

[135] L.-M. Wang and P.J. Steinhardt, *Cluster abundance constraints on quintessence models*, *Astrophys. J.* **508** (1998) 483 [`astro-ph/9804015`] [ɪɴSPIRE].

[136] Y. Gong, *The growth factor parameterization and modified gravity*, *Phys. Rev. D* **78** (2008) 123010 [`arXiv:0808.1316`] [ɪɴSPIRE].

[137] N.-M. Nguyen, D. Huterer and Y. Wen, *Evidence for Suppression of Structure Growth in the Concordance Cosmological Model*, *Phys. Rev. Lett.* **131** (2023) 111001 [`arXiv:2302.01331`] [ɪɴSPIRE].

[138] E.V. Linder and R.N. Cahn, *Parameterized Beyond-Einstein Growth*, *Astropart. Phys.* **28** (2007) 481 [`astro-ph/0701317`] [ɪɴSPIRE].

[139] G.E. Addison et al., *Revisiting the A_L Lensing Anomaly in Planck 2018 Temperature Data*, *Astrophys. J.* **974** (2024) 187 [`arXiv:2310.03127`] [ɪɴSPIRE].